Histone chaperones play crucial roles in maintenance of stem cell niche during plant root development

Jing Ma, Yuhao Liu, Wangbin Zhou, Yan Zhu, Aiwu Dong, Wen-Hui Shen

the plant journal

Histone chaperones play crucial roles in maintenance of stem cell niche during plant root development

Journal:	*The Plant Journal*
Manuscript ID	TPJ-00198-2018.R1
Manuscript Type:	Original Article
Date Submitted by the Author:	27-Mar-2018
Complete List of Authors:	Ma, Jing; Fudan University, Liu, Yuhao; Institute of Plant Biology, School of Life Sciences, Fudan University, State Key Laboratory of Genetic Engineering, International Associated Laboratory of CNRS-Fudan-HUNAU on Plant Epigenome Research, Collaborative Innovation Center for Genetics and Development Zhou, Wangbin; School of life sciences, Fudan University Zhu, Yan; Fudan University, Biochemistry Dong, Aiwu; Fudan University, Biochemistry Shen, Wen-Hui; Institut de Biologie Moléculaire des Plantes du CNRS,
Key Words:	Arabidopsis thaliana, histone chaperone, genome integrity, stem cell maintenance, Root growth

Histone chaperones play crucial roles in maintenance of stem cell niche during plant root development

Jing Ma[1], Yuhao Liu[1], Wangbin Zhou[1], Yan Zhu[1], Aiwu Dong[1,*], Wen-Hui Shen[1,2,*]

[1]State Key Laboratory of Genetic Engineering, Collaborative Innovation Center for Genetics and Development, International Associated Laboratory of CNRS-Fudan-HUNAU on Plant Epigenome Research, Department of Biochemistry, Institute of Plant Biology, School of Life Sciences, Fudan University, Shanghai 200438, PR China

[2]Université de Strasbourg, CNRS, IBMP UPR 2357, F-67000 Strasbourg, France

* To whom correspondence should be addressed:

Wen-Hui Shen

wen-hui.shen@ibmp-cnrs.unistra.fr

Phone: +33 3 67155326

Aiwu Dong

aiwudong@fudan.edu.cn

Phone: +86 21 51630631

Running head: Histone chaperones in stem cell maintenance

Word count: 7601
Figures: 7
Table: 0

SUMMARY

Stem cells in both plant and animal kingdoms reside in a specialized cellular context called stem-cell niche (SCN). SCN integrity is crucial for organism development. Here we show that the H3/H4 histone chaperone CHROMATIN ASSEMBLY FACTOR-1 (CAF-1) and the H2A/H2B histone chaperone NAP1-RELATED PROTEIN1/2 (NRP1/2) play synergistic roles in Arabidopsis root SCN maintenance. Compared to either the *m56-1* double mutant deprived of NRP1 and NRP2 or the *fas2-4* mutant deprived of CAF-1, the combined *m56-1fas2-4* triple mutant displayed a much more severe short-root phenotype. The *m56-1fas2-4* mutant root lost the normal organizing center QC (Quiescent Center), and some initial stem cells differentiate precociously. Microarray analysis unraveled deregulation of 2735 genes within the Arabidopsis genome (representing > 8% of all genes) in the *m56-1fas2-4* mutant roots. Expression of some SCN key regulatory genes (e.g. *WOX5*, *PLT1*, *SHR*) was not limiting rather the plant hormone auxin gradient maximum at QC was impaired. The mutant roots showed programmed cell death and high levels of the DNA damage mark histone H2A.X phosphorylation (γ-H2A.X). Knockout of either *ATM* or *ATR,* encoding a DNA damage response kinase, rescued in part the cell death and the short-root phenotype of the *m56-1fas2-4* mutant. Collectively, our study indicates that NRP1/2 and CAF-1 act cooperatively in regulating proper genome transcription, in sustaining chromatin replication and in maintaining genome integrity, which are crucial for proper SCN function during continuous post-embryonic root development.

Key words: *Arabidopsis thaliana* / histone chaperone / genome integrity / stem cell maintenance / root growth

Significance statement: Concomitant loss of the H3/H4 histone chaperone CAF-1 together with the H2A/H2B histone chaperones NRP1 and NRP2 was found to cause arrest of root growth due to perturbed genome transcription, disorganized stem cell niche, and induced cell death associated with increased nuclear DNA damage.

INTRODUCTION

Continuous plant growth and development is sustained by the small populations of pluripotent stem cells resided in the root and shoot meristems (Heidstra and Sabatini, 2014; Takatsuka and Umeda, 2015). In Arabidopsis root apex, initial stem cells surround the quiescent center (QC), which contains approximately four mitotically inactive cells, together forming the microenvironment, namely the root stem cell niche (SCN). QC functions to prevent the differentiation of surrounding initial stem cells and to maintain their cell fate (van den Berg et al., 1997). The initial stem cells undergo asymmetric cell division to generate self-renewing cells still in contact with QC and its outward daughter cells that give rise to the different cell lineages, namely distal (columella), lateral (lateral root cap and epidermis) and proximal (cortex, endodermis and stele) cell types. After several rounds of mitotic cell division in the meristematic zone, cells increase greatly their volume accompanied by endoreduplication (also named endoreplication) in the elongation zone, and then differentiate to acquire their destined cell fates in the differentiation zone, as marked by emerging root hairs at the epidermal surface.

Cell-type specificities are dictated by genetic information resided within the nucleus in the form of chromatin. Histone chaperones escort nascent histones from cytoplasm to nucleus and participate in nucleosome assembly/disassembly in dynamic chromatin regulation during DNA replication, repair and gene transcription (Avvakumov et al., 2011; Ransom et al., 2010; Zhu et al., 2013). Among them, CHROMATIN ASSEMBLY FACTOR-1 (CAF-1) and NUCLEOSOME ASSEMPLY PROTEIN 1 (NAP1) belong to two distinct families of histone chaperones highly conserved in all eukaryotes including plants (Ramirez-Parra and Gutierrez, 2007b; Zhou et al., 2015). CAF-1 is a heterotrimeric complex acting specifically as a histones H3/H4 chaperone. Arabidopsis CAF-1 is composed of the three subunits FASCIATA1 (FAS1), FAS2 and MULTICOPY SUPPRESSOR OF IRA1 (MSI1). Loss of CAF-1 function in the *fas1* or *fas2* mutant causes many defects including: abnormal shoot and short-root phenotypes associated with meristem dysfunctions (Kaya et al., 2001; Leyser and Furner, 1992), inhibition of mitotic progression and increase of endoreduplication and trichome branching in leaves (Exner et al., 2006; Ramirez-Parra and Gutierrez, 2007a), arrest of generative cell division leading to bicellular instead of normal tricellular pollen formation (Chen et al., 2008), deregulation of genome transcription (Mozgova et al., 2015; Ono et al., 2006; Schonrock et al.,

2006), shortening of telomeres and loss of 45S rDNA (Mozgova et al., 2010; Muchova et al., 2015), increase of both mitotic and meiotic homologous recombination (HR) frequencies (Endo et al., 2006; Gao et al., 2012; Kirik et al., 2006; Varas et al., 2015), and alteration of nucleosome occupancy and H3.1/H3.3 ratio (Jiang and Berger, 2017; Munoz-Viana et al., 2017; Otero et al., 2016).

In contrast to CAF-1, NAP1 functions as a homodimer primarily in chaperoning histones H2A and H2B (Zhou et al., 2015). In Arabidopsis, four genes coding NAP1 (AtNAP1;1 to AtNAP1;4) and two genes coding NAP1-RELATED PROTEIN (NRP1 and NRP2) together form two distinct subfamilies (namely NAP1 and NRP) that display different protein subcellular localization and subfamily-specific dimer formation (Liu et al., 2009a; Zhu et al., 2006). Loss of NAP1 function in the triple mutant *m123* or the quadruple mutant *m1234* results in plant hypersensitivity to abiotic stresses and reduced HR, but does not affect plant growth and development under normal culture conditions (Gao et al., 2012; Liu et al., 2009b; Zhou et al., 2016). Remarkable, loss of both NRP1 and NRP2 in the double mutant *m56* additionally impairs plant root growth (Zhu et al., 2006). A recent study demonstrated that the transcription factor WEREWOLF (WER) recruits NRP1 to activate *GLABRA2* (*GL2*) expression to inhibit root hair formation (Zhu et al., 2017). A previous study showed that chromatin region around *GL2* is more accessible in atrichoblasts (non-root-hair-forming cells) than in trichoblasts (root-hair-forming cells) in the wild-type root and that this cell-type specific chromatin alteration is lost in the *fas2* mutant root (Costa and Shaw, 2006). These studies uncover essential functions of NRP1 and CAF-1 in root epidermal cell fate determinacy. Importantly, however, roles of these histone chaperones in regulation of SCN and root growth remain to be elucidated.

Here, we show that NRP1/2 and CAF-1 act synergistically in maintaining SCN integrity to sustain post-embryonic root growth and development. More specifically, our analyses of the triple mutant *m56-1fas2-4* revealed that depletion of NRPs and CAF-1 causes extremely short-root phenotype because of QC loss associated with genome transcription deregulation, auxin gradient perturbation, cell cycle arrest and cell death at root apex.

RESULTS

Concomitant depletion of NRPs and CAF-1 drastically impairs root growth

Consistent with previous reports (Kaya et al., 2001; Leyser and Furner, 1992; Zhu et al., 2006), loss of either NRP1/NRP2 in the *m56-1* mutant or CAF-1 in the *fas2-4* mutant caused short-root phenotypes (Figure 1A). Our observation of the *m56-1fas2-4* triple mutant (Gao et al., 2012) unraveled that simultaneous loss of NRPs and CAF-1 resulted in drastically enhanced inhibition of root growth. Time course analyses during 12 day-after-germination (DAG) showed that compared to the wild-type (WT) control the *m56-1* and *fas2-4* mutants display significantly reduced rates of primary root growth, whereas the *m56-1fas2-4* mutant almost completely stopped primary root elongation after 5 DAG (Figure 1B). These data indicate that *NRPs* and *CAF-1* act synergistically in promoting plant root growth.

The short-root mutant phenotype is associated with meristem defects

Next, we used plants at 5 DAG to further investigate cellular bases of the mutant root defects. Examination under microscope revealed that the length of root meristem zone is reduced slightly in *m56-1*, severely in *fas2-4* and most drastically in *m56-1fas2-4*, as compared to that of WT (Figure 2A). Consistently, the number of cells in the meristem, defined as the number of cortex cells in a file extending from QC to the first elongated cell (Dello Ioio et al., 2007; Ji et al., 2015), was significantly more reduced in *m56-1fas2-4* as compared to *m56-1* or *fas2-4* (Figure 2B). Thus, a constrained cell division is correlated with the short-root phenotype of these mutants.

Using the mPS–PI (modified Pseudo-Schiff Propidium Iodide) technique (Truernit et al., 2008), we examined the cellular organization at root tip. QC, the central organizer of the root SCN, is surrounded by distinct types of initial cells that ultimately differentiate into functional cell files in the WT root tips. Among them, a single layer of cells functioning as columella initial is located between QC and the differentiated columella cells, which are distinctively marked by starch granules (Figure 2C). The *fas2-4* mutant displayed a disorganized SCN with some initial cells difficult to be firmly defined for their identity. Especially, characteristic feature of cortex/endodermis initial was lost and starch granules extend into cells of the presumptive columella initial layer, indicating a loss of their stem cell identity (Figure 2C). The *m56-1* mutant showed a relatively normal SCN but greatly enhanced *fas2-4* defects in the *m56-1fas2-4* mutant (Figure 2C). Arrangements of stele cells as well as columella cell layers were severely disturbed and the patterning of distinct initial cells was highly irregular rendering the track-back of initial cell identity very difficult in *m56-1fas2-4*. Most strikingly, QC cells in *m56-1fas2-4* were barely

identifiable (Figure 2C). To further verify QC cell fate, we introgressed the *QC25* reporter, which expresses the β-glucuronidase (GUS) gene in QC cells (Sabatini et al., 1999), into our mutant lines. As expected, *QC25* expression was detected specifically in QC cells in WT (Figure 2D). In both *m56-1* and *fas2-4*, *QC25* expression was also detected at QC albeit slightly weaker in *m56-1* and more diffused in *fas2-4* as compared to that in WT. In *m56-1fas2-4*, however, *QC25* expression was undetected (Figure 2D). Staining by Lugol's solution revealed that starch granules accumulate in cells largely beyond columella layers in *m56-1fas2-4* (Figure 2D), suggesting loss of stem cell fate of initial cells. Examination of roots at 15 DAG further confirmed loss of SCN because the *m56-1fas2-4* root tip is mostly occupied by root hair-like cells (Supplemental Figure S1). Taken together, these data clearly indicate that *NRPs* and *CAF-1* act cooperatively in maintaining QC and SCN as well as in promoting cell division and in inhibiting cell differentiation at the root tip.

Loss of NRPs and CAF-1 alters root expression of a large number of genes

To get insight about molecular phenotype of the mutant roots, we performed transcriptome analysis using the Agilent Arabidopsis 4x44K oligonucleotide microarray. Our biological replicates were reproducible in the different mutants as in WT (Supplemental Figure S2). Genes with a changed level of more than two folds in the mutant as compared to WT were considered as differentially expressed. Thus, in total 831 genes in *m56-1*, 1816 genes in *fas2-4*, and 2735 genes in *m56-1fas2-4* were found differentially expressed (Supplemental Datasets 1 to 3), with up-regulated gene numbers slightly higher than down-regulated gene numbers (Figure 3A). The detection of more differentially expressed genes in *m56-1fas2-4* is consistent with the more severe root growth defect of this mutant. Significant overlaps (RF >1 and p-value <0.05) were detected for pairwise comparisons of genes changed in a same direction (up-up or down-down) but not in an opposite direction (up-down or down-up) among the *m56-1, fas2-4* and *m56-1fas2-4* mutants (Figure 3B and 3C, Supplemental Figure S3).

Next, we collected the 3862 genes, which showed differential expression in at least one of the three mutants, and performed *k*-means clustering analysis. Eight clusters comprising varied numbers of genes (Supplemental Dataset 4) were generated (Figure 3D). Among them, Cluster-1 and Cluster-2 represent mostly up-regulated genes in *m56-1fas2-4,* which exhibit good overlap with up-regulated genes in *fas2-4* as well as in *m56-1*. Oppositely, Cluster-7 and

Cluster-8 represent mostly down-regulated genes in *m56-1fas2-4,* which exhibit good overlap with down-regulated genes in *fas2-4* as well as in *m56-1*. These four clusters likely best reflect common regulatory pathways by NRPs/CAF-1 with consistency of the short root phenotypes of the mutants. We then performed gene ontology (GO) analysis on genes belonging to these four clusters. Strikingly, we found that Cluster-1 and Cluster-2 comprise majorly genes involved in RNA and transcription regulation whereas Cluster-7 and Cluster-8 comprise essentially genes involved in stress response and metabolism (Figure 3E). It is noteworthy that our analysis identified several genes previously known as important for root development, including *WOX5* (*WUSCHEL-RELATED HOMEOBOX 5*) (Kong et al., 2015; Sarkar et al., 2007), *ARF5* (*AUXIN RESPONSE FACTOR 5*) (Krogan et al., 2014), *IAA5* (*INDOLEACETIC ACID-INDUCED PROTEIN 5*) and *IAA30* (Sato and Yamamoto, 2008).

Loss of NRPs and CAF-1 affects key regulatory gene expression and auxin gradient at root tip

Quantitative RT-PCR analysis confirmed the transcriptome data showing that transcript levels of several key regulatory genes involved in root growth and patterning are perturbed in *fas2-4* and to a more extend in *m56-1fas2-4* (Figure 4A). To examine chromatin change associated with transcription perturbation, we performed chromatin immunoprecipitation (ChIP) analysis using specific antibodies against H3, acetylated H3 (H3ac) or acetylated H4 (H4ac). As shown in Figure 4B, levels of H3 enrichment at all examined genes were similar in *m56-1*, *fas2-4* and *m56-1fas2-4* as in WT. Interestingly, levels of both H3ac and H4ac were increased in *fas2-4* and to a more extend in *m56-1fas2-4* as compared to WT, as observed at *WOX5*, *ARF5*, *1AA30* and *SHORT ROOT* (*SHR*) but not at *SCARECROW* (*SCR*). This is consistent with increased transcription of *WOX5*, *SHR*, *ARF5* and *1AA30* but not *SCR*.

WOX5 encodes a key homeodomain transcription factor involved in maintaining stem cell identity in the root initials surrounding the QC (Kong et al., 2015; Sarkar et al., 2007). Next, we introgressed the *WOX5:GFP* reporter, which encodes the green fluorescent protein (GFP) driven by the *WOX5* promoter (Blilou et al., 2005), into our mutants. In WT as well as in *m56-1* and *fas2-4*, GFP signals from *WOX5:GFP* expression were detected specifically in QC cells. Interestingly, in *m56-1fas2-4* strong GFP signals were detected in the presumptive position of vascular initial cells and columella initial cells (Figure 4C). A previous study showed that

ectopic *WOX5* expression could block the differentiation of columella stem cell descendants (Sarkar et al., 2007). However, our staining with mPS–PI and Lugol's solution clearly indicated that the presumptive columella stem cells in *m56-1fas2-4* have obviously differentiated as revealed by the accumulated starch granules (Figure 2C and 2D). It is likely that *NRPs* and *CAF-1* act independently from *WOX5*. In support of this, the differentiation-promoting transcription factor gene *CDF4* (*CYCLING DOF FACTORS 4*), which represents a direct target gene repressed by WOX5 (Pi et al., 2015), was found expressed at similar levels in the mutants as in WT (Figure 4A). Moreover, a previous study also showed that distal stem cell differentiation could be triggered in a WOX5-independent manner (Richards et al., 2015).

In addition to *WOX5*, *SHR* and *SCR* act in a parallel pathway with *PLETHORA1* (*PLT1*) to maintain QC identity and stem cell homeostasis in the Arabidopsis root (Aida et al., 2004). While *PLT1* and *SCR* transcript levels remained similarly in *m56-1fas2-4* as in WT, *SHR* was found up-regulated in *fas2-4* and *m56-1fas2-4* (Figure 4A). Since SCR functions downstream of SHR, we introgressed the *pSCR:SCR-GFP* reporter encoding GFP fused in frame with the C-terminus of SCR (Gallagher et al., 2004) into our mutants. We detected a cup-like pattern of SCR-GFP signals surrounding stele in longitudinal sections of all mutant roots similarly as that of WT, excepting that in *m56-1fas2-4* the signal is slightly weaker (Figure 4D). Thus, the SHR/SCR and PLT1 pathways are relatively well conserved in the absence of NRPs and CAF-1.

The phytohormone auxin plays key roles in plant root development. *ARF5*, encoding an important transcriptional regulator of various Aux/IAA genes (Krogan et al., 2014), was up-regulated in both *fas2-4* and *m56-1fas2-4* (Figure 4A). Consistently, the transcription levels of *IAA5* and *IAA30*, the direct target genes of *ARF5*, were also significantly enhanced. The other auxin response factor genes *ARF12* and *ARF21* were down-regulated (Figure 4A). To get insight about auxin distribution, the auxin-response reporter *DR5rev:GFP* (Friml et al., 2003) was introgressed into our mutants. The reporter was found to be expressed as a polar gradient in columella cells and showed a maximum of accumulation in the QC cells in the WT and *m56-1* roots, and slightly less obvious in the *fas2-4* roots (Figure 4E). In *m56-1fas2-4* roots, however, the expression level of *DR5rev:GFP* was drastically reduced and the pattern of maximum in QC position was mostly lost (Figure 4E). It is likely that perturbed auxin regulatory pathways are associated with root developmental defects of the *m56-1fas2-4* mutant.

Based on our data, we conclude that the root SCN disorganization in *m56-1fas2-4* is not primarily caused by any lack of WOX5/SHR/SCR/PLT key regulators but is rather associated with a perturbed regulation of auxin homeostasis critical for cell division and cell-fate determinacy.

NRPs and CAF-1 promote mitotic cell division and inhibit endocycles

To provide insight about cell proliferation and cell differentiation, we first evaluated expansion rate of epidermal cells following their development out from initial stem cells. A plot of epidermal cell area against the distance from QC revealed that *m56-1* and *fas2-4* epidermal cell expansion occurred at slightly higher rates than did WT. In comparison, the cell expansion was much more pronounced in *m56-1fas2-4* (Figure 5A). Cell enlargement frequently is associated with endoreduplication. We next performed flow cytometry analysis to measure the nuclear polyploidy levels in the roots. In WT, the nuclear ploidy level of 2C cells was found at higher percentage than 4C and 8C cells, whereas 16C cells only reached less than 6%. In all mutants, the percentage of 2C cells was reduced whereas those of higher ploidy level cells were increased at varied degrees. The *m56-1fas2-4* mutant showed highest increase of polyploidy levels, with 16C cells reaching proximately to 10% (Figure 5B). Thus, in contrast to cell number reduction associated with the short-root phenotype, cell size is increased together with enhanced endoreduplication in the *m56-1fas2-4* mutant primary root.

Endocycle differs from a canonical cell cycle by successive duplication of genomic DNA without mitotic chromosome segregation. To further investigate the cell cycle, we introgressed the *cyclin-GUS* reporter encoding GUS fused in frame at C-terminus of CYCB1;1 (Colon-Carmona et al., 1999) into our mutant lines. The cyclin gene *CYCB1;1* is induced upon entry into G2 phase of the cell cycle and acts in promoting mitosis (M phase) progression. In agreement with previous studies (Endo et al., 2006; Zhu et al., 2006), we found that GUS positive cells are increased in the *m56-1* mutant root and to a more extent in the *fas2-4* mutant root as compared to the WT root. Most remarkably, compared to either *m56-1* or *fas2-4* the *m56-1fas2-4* mutant root showed an enhanced increase of GUS positive cells (Figure 5C). This indicates that many cells are arrested before G2/M transition to exit mitotic cycle to enter endocycle. Quantitative RT-PCR analysis confirmed higher levels of expression of *CYCB1;1* as well as *CYCB1;3* and *CYCB1;4* in *m56-1fas2-4* (Figure 5D). It is likely that expression of

mitotic regulators was not rate limiting, rather that a slow-down of nucleosome assembly, caused by lack of the CAF-1 and NRP histone chaperones, had lengthened G2 and favored cell differentiation accompanied by endoreduplication in the mutant roots.

NRPs and CAF-1 prevents programmed cell death in root tips

The *m56-1fas2-4* mutant also showed synergistic increase of expression of several genes involved in DNA damage checkpoint or repair (Figure 5D), including the cyclin-dependent kinase inhibitor gene *SMR5*, the kinase gene *WEE1* and the transcription factor gene *SOG1* as well as *POLY ADP-RIBOSE POLYMERASE 1*(*PARP1*), *PARP2*, *RADIATION SENSITIVE 51*(*RAD51*), *RAD54* and *BREAST CANCER SUSCEPTIBILITY 1*(*BRCA1*) (Hu et al., 2016). DAPI (4',6-diamidino-2-phenylindole) staining did not detect any significant abnormality of nuclei of cells around QC (Supplemental Figure S4). It is known that DNA damage, such as double strand break (DSB), can induce early onset of endoreduplication in the transition zone of root epidermis (Adachi et al., 2011). We further used PI-staining, which specifically marks dead cells because of impaired membrane integrity, to evaluate cell death at root apex. Dead cells were undetected in the WT or *m56-1* root tips, but clearly detected in the *fas2-4* and to a more extent in the *m56-1fas2-4* root tips (Figure 6A). Cell death occurred in 43% percent of the *fas2-4* root tips (n=42) as compared to about 90% of the *m56-1fas2-4* root tips (n=51) (Figure 6B). In addition, we also quantified the level of cell death by measuring the size of total PI-stained speckles per root. Our data showed again an increased degree of cell death in *m56-1fas2-4* (600 μm^2 on average, n=65) as compared to that in *fas2-4* (370 μm^2 on average, n=65) (Figure 6B). The observed cell death has occurred primarily in distal stem cells into the meristematic zone.

Cell death in *m56-1fas2-4* is partly dependent on the ATM and ATR pathways

Two closely related kinases, ATAXIA-TELANGIECTASIA MUTATED (ATM) and ATM/RAD3-RELATED (ATR), are involved in plant response to DNA damage (Hu et al., 2016). ATM responds to DSB mediating transcriptional activation of genes involved in DNA repair (Shiloh, 2006), and ATR mainly responds to replication folk stagnation-induced DNA breaks and has an accessory role in transcriptional regulation after irradiation (Culligan et al., 2006; Richards et al., 2015). To investigate whether DNA damage causes cell death and root growth arrest, we generated the *atm-2m56-1fas2-4* and *atr-2m56-1fas2-4* quadruple mutants. Indeed, compared to *m56-1fas2-4*, both the *atm-2m56-1fas2-4* and *atr-2m56-1fas2-4* quadruple

mutants showed alleviated cell death (Figure 6) and ameliorated root growth (Supplemental Figure S5).

Upon DSB occurrence, histone variant H2A.X at the DSB site is quickly phosphorylated by ATM/ATR, resulting in γ-H2A.X (Friesner et al., 2005). To provide evidence for the role of ATM and ATR at the molecular level, we performed both whole-mount root immunostaining and western blot analyses to check γ-H2A.X levels in the different mutants. Under normal growth conditions, the *m56-1fas2-4* mutant root-tip and to a less extent the *fas2-4* mutant root-tip showed clearly detectable immunostaining signals of γ-H2A.X (Figure 7A). In contrast, γ-H2A.X staining signal was barely detectable in WT, *m56-1*, *atm-2*, *atm-2m56-1fas2-4*, *atr-2*, and *atr-2m56-1fas2-4* (Figure 7A). Western blot analysis revealed that global levels of H3 and H2A remain largely unchanged in *m56-1*, *fas2-4* and *m56-1fas2-4* as compared to WT (Figure 7B). γ-H2A.X was detected in *fas2-4* and to a higher level in *m56-1fas2-4* (Figure 7C), but was undetected in WT, *m56-1*, *atm-2*, *atm-2m56-1fas2-4*, *atr-2*, and *atr-2m56-1fas2-4* (Figure 7C,D).

We further examined γ-H2A.X levels using plants after treatment with bleomycin, a genotoxin efficiently inducing DSB (Lloyd et al., 1978). Western blot data (Figure 7E,F,G)showed that bleomycin-treatment induced γ-H2A.X elevation in WT and in all mutants excepting *atm-2* and *atm-2m56-1fas2-4*, the two mutants where γ-H2A.X remained undetected. This is consistent with the crucial role of ATM in H2A.X phosphorylation and DSB repair (Friesner et al., 2005; Hu et al., 2016). In addition, albeit to a less extend ATR also played a role in bleomycin-induced H2A.X phosphorylation because *atr-2* and *atr-2m56-1fas2-4* showed reduced levels of γ-H2A.X as compared to WT and to *m56-1fas2-4*, respectively (Figure 7G). Since *atr-2m56-1fas2-4* displayed a root growth performance similarly or even better than did *atm-2m56-1fas2-4* (Supplemental Figure S5), we conclude that depletion of NRPs/CAF-1 activates both γ-H2A.X/DSB-responsive and replication folk stagnation-responsive pathways, the two major pathways coordinating cell proliferation, endocycle, DNA repair and cell death (Hu et al., 2016).

DISCUSSION

In this study, we demonstrated that the histone chaperones NRPs and CAF-1 synergistically act in maintaining SCN organization and function during plant post-embryonic root development. In line with fundamental roles of histone chaperones in nucleosome assembly, depletion of NRPs and CAF-1 was found to impede chromatin-based processes, including transcription, DNA replication and repair, which mutually contribute to root anomaly phenotype of the *m56-1fas2-4* mutant. In the mutant root apex, QC was abrogated, and its surrounding stem cells tended to lose the short-range inhibition from QC and improperly underwent cell differentiation. Intriguingly, this mutant SCN defect occurred in a manner independent of WOX5, a QC-specific transcription factor generally recognized as the key repressor of stem cell differentiation (Heidstra and Sabatini, 2014; Kong et al., 2015; Sarkar et al., 2007; Takatsuka and Umeda, 2015). The *m56-1fas2-4* mutant roots exhibited deregulation of a large number of genes as well as severe cell death, high level of endoreduplication and premature of cell differentiation, pointing to a rapid exhaustion of transit-amplifying stem cells. In the absence of NRPs and CAF-1, the plant genome became more instable and vulnerable to DSB damage, as evidenced by increase of γ-H2A.X in the *m56-1fas2-4* mutant roots. Interestingly, *atm-2* and also *atr-2* could partly rescue the *m56-1fas2-4* mutant defect, e.g. γ-H2A.X accumulation, cell death and root growth inhibition, unraveling an effective role of the ATM and ATR signaling pathway to link genome integrity with stem cell function.

Transcriptome analysis revealed more important number of deregulated genes in *m56-1fas2-4* than in *fas2-4* and further than in *m56-1*, which is in good correlation with the gradual severity of root growth defects displayed by these mutants. Importantly, a statistically significant overrepresentation of commonly deregulated genes was detected in the three mutants, supporting a concerted action together between the H2A/H2B-chaperone NRP1/2 and the H3/H4-chaperone CAF-1 in nucleosome assembly. Histone chaperone can directly participate in transcription regulation of target genes through local nucleosome dynamics, in which histone barrier to RNA Polymerase is released or aggravated by chaperone activities (Zhou et al., 2015). During epidermal cell fate determination in Arabidopsis roots, NRP1 interacts with the MYB-domain transcription factor WER and is enriched at the promoter region of *GL2* to mediate its full expression level in a WER-dependent manner (Zhu et al., 2017). CAF-1 has been reported to be involved in restoration of heat-induced transcriptional silencing of repetitive

elements during Arabidopsis plant recovery from heat stress (Pecinka et al., 2010). Depletion of CAF-1 broadly affects genome transcription (Mozgova et al., 2015; Ono et al., 2006; Schonrock et al., 2006; this study). Low nucleosome occupancy (Mozgova et al., 2015) and high levels of H3/H4 acetylation (Ramirez-Parra and Gutierrez, 2007a; this study) were found to be associated with up-regulation of genes in the *fas* mutants. Remarkably, simultaneous loss of CAF-1 and NRPs further enhanced H3/H4 acetylation and transcription levels of *WOX5*, *ARF5*, *1AA30* and *SHR* in *m56-1fas2-4*, suggesting that these two types of histone chaperones act synergistically. A synergistic as well as an additive function between CAF-1 and NRPs may explain the higher number of deregulated genes found in *m56-1fas2-4* than in *fas2-4* and *m56-1*. Future studies are still necessary to investigate more precisely the molecular mechanisms underlying both activation and repression of gene transcription by histone chaperones.

Many transcription factor genes were found deregulated, which may also partly contribute, through secondary effects, to the observed high number of differentially expressed genes in our mutants. Intriguingly, some well-studied root patterning genes such as *PLT1* and *SCR* have largely maintained their wild-type transcriptional level in the mutants. Moreover, the reporter gene *pSCR:SCR-GFP* exhibits nearly normal expression pattern in *m56-1fas2-4* as well as in *m56-1* and *fas2-4*. A related marker *proSCR:GFP* was previously examined in *fas1-1* in En (Enkhelm) ecotype, and showed ectopic expression in cell layer not in contact with stele as well as absence of expression in random cell(s) in proper cell layer (Kaya et al., 2001). Thus, the requirement for CAF-1 in *SCR* expression seems to be ecotype specific. Similar situation had also been found in transcription factor *GL2* and cell fate determination of epidermal cells, e.g. ectopic expression of *GL2* and impaired root hair phenotype were observed in *fas2* allele in the L*er* background but not in *fas2-4* in Col background (Zhu et al., 2017). In contrast, while unexamined under L*er* background, under Col background the *m56-1fas2-4* mutant showed absence of GUS staining from the QC-specific marker *QC25* and loss of QC as well as drastic reduction of the auxin gradient maximum in QC position, as detected by the *DR5rev:GFP* distribution pattern. Ectopic expression of *IAA30* has been reported to cause collapse of root apical meristem (Sato and Yamamoto, 2008), thus our observed increase of *IAA30* expression could be nicely associated with the mutant root phenotype in *m56-1fas2-4*. Moreover, expression of *WOX5* was found increased in *m56-1fas2-4*, which is in agreement with that auxin acts as a

repressor upstream of *WOX5* transcription (Ding and Friml, 2010). Interestingly, a dynamic change of H3.1/H3.3 levels was observed in QC cells during embryogenesis, showing a high level of H3.1 at early stage when *WOX5* starts to express and a replacement of H3.1 by H3.3 at late embryo stage (Otero et al., 2016). CAF-1, acting as an H3.1-specific chaperone (Ramirez-Parra and Gutierrez, 2007b), might have been involved in this process in regulating QC cell fate and *WOX5* expression. Depletion of the SWI2/SNF2-family ATP-dependent chromatin remodeling factors CHR12 and CHR23 has also been found to cause a loss of *QC25* expression in QC position and a reduced *DR5rev:GFP* expression but an expanded *proWOX5:GFP* expression in root apex (Sang et al., 2012). Considering that histone chaperones frequently act together with ATP-dependent chromatin remodeling factors in nucleosome assembly/disassembly (Zhou et al., 2015), it is reasonable to speculate that CHR12/CHR23 and NRPs/CAF-1 may share common regulatory pathways in root developmental regulation. Nonetheless, increased *WOX5* expression cannot be taken as a cause of QC abrogation because *WOX5* overexpression inhibits differentiation of columella cells and only its loss-of-function results in abrogation of QC cells (Sarkar et al., 2007). WOX5-independent pathways (Richards et al., 2015) might have been implicated in the CHR12/CHR23 chromatin remodeling and the NRPs/CAF-1 histone chaperone regulation of SCN function during post-embryonic root development.

In a previous study, it has been shown that more DSB damage occurred in *m56-1fas2-4* than in *m56-1* or *fas2-4,* at either normal or bleomycin-treated plant growth conditions (Gao et al., 2012). In the current study, we used DSB molecular marker γ-H2A.X and confirmed the highly severe chromatin instability in root cells of *m56-1fas2-4*. More importantly, many γ-H2A.X signals were found in meristematic cells proximal to SCN, pointing to specific deficiency of the *m56-1fas2-4* mutant in maintaining genome integrity during rapid DNA replication and cell proliferation. As a possible consequence of genome damage, cell death and endoreduplication were triggered in high frequency, which may serve to avoid risks of transmission of genetic mutation from stem cells into daughter cells. Maintenance of stem cell feature and meristem cell division capacity are crucial to root development, and it is thus reasonable to speculate that severe chromatin instability has contributed to the disordered root meristem and patterning, which in turn cause root growth defects in *m56-1fas2-4*. In line with

this idea, knockout of either *ATM* or *ATR* function significantly alleviated γ-H2A.X accumulation and cell death as well as root growth inhibition in the *atm-2m56-1fas2-4* or *atr-2m56-1fas2-4* mutant. This latter observation also indicates that ATM and ATR signaling pathways act downstream of DNA damage (DSB and replication folk stagnation) induced by depletion of histone chaperones. The *fas* mutants display several chromosomal abnormalities including formation of chromatid bridges and acentric fragments detected in young flower bud cells (Varas et al., 2017), increase of somatic and meiotic HR frequencies (Endo et al., 2006; Gao et al., 2012; Kirik et al., 2006; Varas et al., 2015), and shortening of telomeres and loss of 45S rDNA (Mozgova et al., 2010; Muchova et al., 2015) . Previous investigation of *m56-1fas2-4* has revealed that *m56-1* is epistatic to *fas2-4* in somatic HR but hypostatic to *fas2-4* in telomere length regulation (Gao et al., 2012). These types of genetic interaction differ from the synergistic interaction between *m56-1* and *fas2-4* in γ-H2A.X and cell death induction. Future work will be necessary to address whether or not a specific chromosomal abnormality is more closely linked with cell death and how ATM/ATR-mediated γ-H2A.X contributes to chromosomal abnormalities caused by histone chaperone depletion.

Lastly, the synergistic interaction between *m56-1* and *fas2-4* in root growth inhibition also differs from the epistatic role of *fas2-4* over *m56-1* in shoot growth regulation, as *m56-1fas2-4* showed a mutant phenotype of aerial organs similar to that of *fas2-4* (Gao et al., 2012). Such difference might not be ascribed to distinct cell-type-specific expression patterns because *NRP1/2* and *FAS* genes are ubiquitously expressed in whole plant. Similar to *WOX5* in roots *WUSCHEL* (*WUS*) in shoot plays a conserved role in SCN function, yet differences exist, at both up and downstream, in regulation between *WOX5* in root and *WUS* in shoot (Heidstra and Sabatini, 2014; Sarkar et al., 2007). Moreover, the *m56-1fas2-4* mutant root phenotype is majorly associated to WOX5-independent regulation pathways. The root and shoot SCN may also have distinct protection to DNA damage linked with different functions of histone chaperones. Finally, NRP1/2 function in shoot may be fully redundant and masked by AtNAP1, the homologous H2A/H2B-chaperone encoded by four genes in Arabidopsis (Liu et al., 2009a; Zhu et al., 2006). These different assumptions intrigue future interest to investigate precise function of the H2A/H2B-chaperone NRP1/2 and the H3/H4-chaperone CAF-1 in Arabidopsis shoot SCN regulation. The rice CAF-1 has also been shown to be required for normal shoot

apical meristem (SAM) development (Abe et al., 2008). Strikingly, however, in contrast to the Arabidopsis *fas* mutants where loss of CAF-1 increased SAM size (Kaya et al., 2001; Leyser and Furner, 1992), the rice *caf-1* (*fsm*) mutant displayed a reduced SAM (Abe et al., 2008). Very likely, different plant species deploy varied molecular mechanisms in regulation of SCN function and maintenance.

EXPERIMENTAL PROCEDURES

Plant materials and growth conditions

The WT and mutant Arabidopsis lines used in this study are all in Columbia (Col) ecotype background. The reporter lines *proWOX5:GFP, proSCR:SCR-GFP, DR5rev:GFP,CYCB1;1:GUS* and *QC25* have been described in previous studies (Blilou et al., 2005; Colon-Carmona et al., 1999; Gallagher et al., 2004; Sabatini et al., 1999). Higher order combinations of mutants were generated by genetic crosses. For root analysis, seedlings were grown on MS plates containing agar-solidified medium M0255 (Duchefa, http://www.duchefa.com), 2% sucrose and 0.9% agar, pH 5.7 at 22°C under 16 h light/8 h dark photoperiod.

GUS and Lugol staining

For GUS staining, 5-day-old seedlings were incubated for 3–4 hours at 37°C in a solution containing 0.04% 5-bromo-4-chloro-3-indolyl-β-D-glucuronide, 21.2 mM NaH_2PO_4, 28.8 mM Na_2HPO_4, 2 mM $K_4Fe(CN)_6$, 2 mM $K_3Fe(CN)_6$, 5 mM EDTA, and 0.1% Triton X-100. For Lugol starch granule staining, roots were immersed in Lugol iodine solution containing 5% iodine for 2 min. After washing, roots were cleared with chloral hydrate solution (chloral hydrate: water: glycerol, 8:3:1, w/v/v). Approximately 50 to 60 seedlings for each line were examined in at least three independent experiments. DIC (Differential Interference Contrast) images were acquired with an Imager A2 microscope (Zeiss, http://microscopy.zeiss.com).

DAPI staining, PI/ mPS–PI staining and confocal microscopy

For DAPI staining, 5-day-old seedlings were first fixed in the presence of 1% triton in the MTSB buffer (50 mM PIPES, 5 mM EGTA, 5 mM $MgSO_4$, pH 7.0) for 2 hours, then washed with the MTSB buffer, and finally incubated in DAPI solution. Epiflurescence microscopy was

performed for DAPI staining image under UV light. Nuclear area was measured using IMAGE-J software. The mPS-PI staining was performed according to the previously described method (Truernit et al., 2008). Briefly, plant roots were immersed in staining solution containing 10 μg/ml propidium iodide (Sigma, http://www.sigmaaldrich.com) for 30 seconds. Confocal image analysis was performed using a LSM710 microscope (Zeiss) with the following excitation/emission wavelengths: 561 nm/591 to 635 nm for PI, 488 nm/505 to 530 nm for GFP. The area of cell death was quantified by IMAGE-J software. All images were counted from at least 60 plants, and the experiments were repeated three times.

Flow cytometry

To determine ploidy level, flow cytometry was performed as previously described (Larson-Rabin et al., 2009) using roots of over 300 individual 5-day-old seedlings per line. Approximately 15,000 nuclei per sample were analyzed and three independent biological replicates were performed. The KaleidaGraph 4.03 software was used in the non-parametric variant of the t-test (Mann-Whitney test) for assessment of statistical significance.

Microarray

Twelve-day-old plant roots (5 mm from tip) were collected for transcriptome analyses. RNA was extracted using the TRIzol kit according to the manufacturer's instructions (Invitrogen). The microarrays experiment of two biological replicates of WT and three mutants were performed by using the Agilent Arabidopsis 4x44K oligonucleotide array (Shanghai Biotechnology Corporation, www.shbiotech.org). The raw data of microarray have been deposited in public database NCBI-GEO (GSE81229). The online bioinformatics analysis platform called SBC Analysis System (SAS, http://www.shanghaibiotech.com/sas.html) was used to identify differential expressed probes and gene annotation. Genes whose expressions changed more than two-fold between WT and mutant and whose flag value in all sample only appear A one time were considered as differentially expressed. Lists of genes differentially expressed in the different mutants were compared in Venn diagrams generated using VENNY 2.1 (http://bioinfogp.cnb.csic.es/tools/venny). The representation factor and statistical significance of the observed overlap were determined with a hypergeometric test using the Web-based calculator developed by Jim Lund at the University of Kentucky (http://nemates.org/MA/progs/overlap_stats.html). A representation factor (RF) superior to 1 and *p*-value inferior to 0.05

indicate more overlap than expected between two groups at random. K-means clustering was used to cluster deregulated genes into eight groups based on changes in gene expression among mutants, and heatmap was generated with "Complex Heatmap" packages (Gu et al., 2016). For the gene ontology (GO) enrichment analysis, we uploaded the genes to the online tool GOEAST (http://omicslab.genetics.ac.cn/GOEAST/php/agilent.php), which had been proven to provide unbiased GO analysis for high-throughput experimental results, especially for results from microarray hybridization experiments (Wang et al., 2015). The significantly enriched biological processes and molecular function among the genes (p <0.05) were identified.

Quantitative RT–PCR

Roots (5 mm from tip) of over 100 individual 12-day-old plants were harvested, and RNA was isolated using the TRIzol kit according to standard procedures (Invitrogen, http://www.invitrogen.com). Reverse transcription was performed using Improm-II reverse transcriptase (Promega, http://www.promega.com). Quantitative RT-PCR was performed from the cDNA template using gene-specific primers as listed in the supplemental Table S1. *ACTIN2* was used as a reference gene to normalize the data. Three biological replicates of each sample and three technical (PCR) replicates were performed.

Chromatin immunoprecipitation (ChIP)

ChIP analysis was performed as previously described (Bu et al., 2014). Antibodies used in this analysis were anti-H3 (05-499; Millipore, http://www.merckmillipore.com), anti-acetyl (K9 + K14 + K18 + K23 + K27) H3 (ab47915; abcam, http://www.abcam.com), and anti-acetyl (K5 + K8 + K12 + K16) H4 (ab10807; abcam). Gene-specific primers used in quantitative real-time PCR were listed in supplemental Table S1.

Whole-mount root immunostaining and γ-H2A.X detection

Immunofluorescence staining was performed according to the previously described method (Muller et al., 1998). Briefly, 3-day-old seedlings were fixed in 4% formaldehyde in MTSB (50 mM PIPES, 5 mM EGTA, 5 mM $MgSO_4$, pH 7.0) and treated with Driselase (Sigma) at 37°C for 3 hours. After washing with MTSB, the samples were incubated in blocking buffer (1xPBS containing 1% BSA) at room temperature for 2 hours. Then samples were incubated with the γ-H2A.X antibody (Zhou et al., 2016) at 4°C overnight. Alexa Fluor 555-conjugated anti-rabbit IgG antibodies (A21428, Invitrogen) were used as the second antibody. After DAPI staining,

imaging was performed using the LSM710 confocal microscope. All staining, imaging and processing conditions are strictly the same for the WT and the different mutants.

Western blot analysis

Twelve-day-old plants were incubated in liquid MS supplemented with or without 2 μM bleomycin for 6 h and then harvested for roots. Proteins were extracted as previously described (Yu et al., 2004) in a modified extraction buffer containing in addition 20 mM NaF, an inhibitor of phosphatase. The protein extracts were separated on 15% SDS-PAGE gel and transferred onto a polyvinylidene fluoride membrane (Millipore). The membrane was blotted with anti-ACTIN (ab197345, abcam; 1:1000 dilution), anti-γ-H2A.X (1:500 dilution) and anti-H3 (1:2000 dilution) antibodies, and signals were detected using the enhanced chemiluminescence kit according to the manufacturer's instructions (GE Healthcare, http://www.gelifesciences.com).

ACKNOWLEDGMENTS

We thank the Arabidopsis Biological Resource Centre (ABRC) for providing Arabidopsis seeds. This research work was conducted within the context of the International Associated Laboratory Plant Epigenome Research, LIA PER.

COMPETING INTERESTS

The authors declare no competing or financial interests.

AUTHOR CONTRIBUTIONS

W.H.S. and A.D. planned and designed the research. J.M., Y.L. and W.Z. performed experiments and analyzed data. Y.Z. provided technical assistance and helped in data analysis. W.H.S., J.M. and Y.Z. wrote the manuscript. All authors have seen and approved the manuscript.

FUNDING

This work was supported by National Basic Research Program of China (973 Program, grants no. 2012CB910500) and National Natural Science Foundation of China (grant numbers 31571319, 31570315, 31671341, 91519308 and 31371304).

SUPPLEMENTARY INFORMATION

Supplemental Figure S1. Root phenotype analysis showing drastically disorganization of root apex in the *m56-1fas2-4* mutant.

Supplemental Figure S2. Comparisons of microarray data sets obtained in this study.

Supplemental Figure S3. Venn diagrams showing pairwise overlap together with statistic significance assessment between lists of genes differentially expressed in the *m56-1*, *fas2-4*, and *m56-1fas2-4* mutants.

Supplemental Figure S4. DAPI-staining analysis of nuclei of cells around QC in WT and in the *m56-1*, *fas2-4*, and *m56-1fas2-4* mutants.

Supplemental Figure S5. Loss of *ATM* or *ATR* partially rescues the short root phenotype of the *m56-1fas2-4* mutant.

Supplemental Dataset 1. List of differentially expressed (up-regulated and down-regulated) genes in *m56-1*.

Supplemental Dataset 2. List of differentially expressed (up-regulated and down-regulated) genes in *fas2-4*.

Supplemental Dataset 3. List of differentially expressed (up-regulated and down-regulated) genes in *m56-1fas2-4*.

Supplemental Dataset 4. Expression level change of genes belonging to the different *k*-means clusters (C1 to C8) in the *m56-1*, *fas2-4* and *m56-1fas2-4* mutants.

Supplemental Table S1. List of primers used in this study.

REFERENCES

Abe, M., H. Kuroshita, M. Umeda, J. Itoh, and Y. Nagato. 2008. The rice flattened shoot meristem, encoding CAF-1 p150 subunit, is required for meristem maintenance by regulating the cell-cycle period. *Dev Biol*. 319:384-393.

Adachi, S., K. Minamisawa, Y. Okushima, S. Inagaki, K. Yoshiyama, Y. Kondou, E. Kaminuma, M. Kawashima, T. Toyoda, M. Matsui, D. Kurihara, S. Matsunaga, and M. Umeda. 2011. Programmed induction of

endoreduplication by DNA double-strand breaks in Arabidopsis. *Proc Natl Acad Sci U S A*. 108:10004-10009.

Aida, M., D. Beis, R. Heidstra, V. Willemsen, I. Blilou, C. Galinha, L. Nussaume, Y.S. Noh, R. Amasino, and B. Scheres. 2004. The PLETHORA genes mediate patterning of the Arabidopsis root stem cell niche. *Cell*. 119:109-120.

Avvakumov, N., A. Nourani, and J. Cote. 2011. Histone chaperones: modulators of chromatin marks. *Mol Cell*. 41:502-514.

Blilou, I., J. Xu, M. Wildwater, V. Willemsen, I. Paponov, J. Friml, R. Heidstra, M. Aida, K. Palme, and B. Scheres. 2005. The PIN auxin efflux facilitator network controls growth and patterning in Arabidopsis roots. *Nature*. 433:39-44.

Bu, Z., Y. Yu, Z. Li, Y. Liu, W. Jiang, Y. Huang, and A.W. Dong. 2014. Regulation of arabidopsis flowering by the histone mark readers MRG1/2 via interaction with CONSTANS to modulate FT expression. *PLoS Genet*. 10:e1004617.

Chen, Z., J.L. Tan, M. Ingouff, V. Sundaresan, and F. Berger. 2008. Chromatin assembly factor 1 regulates the cell cycle but not cell fate during male gametogenesis in Arabidopsis thaliana. *Development*. 135:65-73.

Colon-Carmona, A., R. You, T. Haimovitch-Gal, and P. Doerner. 1999. Technical advance: spatio-temporal analysis of mitotic activity with a labile cyclin-GUS fusion protein. *Plant J*. 20:503-508.

Costa, S., and P. Shaw. 2006. Chromatin organization and cell fate switch respond to positional information in Arabidopsis. *Nature*. 439:493-496.

Culligan, K.M., C.E. Robertson, J. Foreman, P. Doerner, and A.B. Britt. 2006. ATR and ATM play both distinct and additive roles in response to ionizing radiation. *Plant J*. 48:947-961.

Dello Ioio, R., F.S. Linhares, E. Scacchi, E. Casamitjana-Martinez, R. Heidstra, P. Costantino, and S. Sabatini. 2007. Cytokinins determine Arabidopsis root-meristem size by controlling cell differentiation. *Curr Biol*. 17:678-682.

Ding, Z., and J. Friml. 2010. Auxin regulates distal stem cell differentiation in Arabidopsis roots. *Proc Natl Acad Sci U S A*. 107:12046-12051.

Endo, M., Y. Ishikawa, K. Osakabe, S. Nakayama, H. Kaya, T. Araki, K. Shibahara, K. Abe, H. Ichikawa, L. Valentine, B. Hohn, and S. Toki. 2006. Increased frequency of homologous recombination and T-DNA integration in Arabidopsis CAF-1 mutants. *EMBO J*. 25:5579-5590.

Exner, V., P. Taranto, N. Schonrock, W. Gruissem, and L. Hennig. 2006. Chromatin assembly factor CAF-1 is required for cellular differentiation during plant development. *Development*. 133:4163-4172.

Friesner, J.D., B. Liu, K. Culligan, and A.B. Britt. 2005. Ionizing radiation-dependent gamma-H2AX focus formation requires ataxia telangiectasia mutated and ataxia telangiectasia mutated and Rad3-related. *Mol Biol Cell*. 16:2566-2576.

Friml, J., A. Vieten, M. Sauer, D. Weijers, H. Schwarz, T. Hamann, R. Offringa, and G. Jurgens. 2003. Efflux-dependent auxin gradients establish the apical-basal axis of Arabidopsis. *Nature*. 426:147-153.

Gallagher, K.L., A.J. Paquette, K. Nakajima, and P.N. Benfey. 2004. Mechanisms regulating SHORT-ROOT intercellular movement. *Curr Biol*. 14:1847-1851.

Gao, J., Y. Zhu, W. Zhou, J. Molinier, A. Dong, and W.H. Shen. 2012. NAP1 family histone chaperones are required for somatic homologous recombination in Arabidopsis. *Plant Cell*. 24:1437-1447.

Gu, Z., R. Eils, and M. Schlesner. 2016. Complex heatmaps reveal patterns and correlations in multidimensional genomic data. *Bioinformatics*. 32:2847-2849.

Heidstra, R., and S. Sabatini. 2014. Plant and animal stem cells: similar yet different. *Nat Rev Mol Cell Biol*. 15:301-312.

Hu, Z., T. Cools, and L. De Veylder. 2016. Mechanisms Used by Plants to Cope with DNA Damage. *Annu Rev Plant Biol*. 67:439-462.

Ji, H., S. Wang, K. Li, D. Szakonyi, C. Koncz, and X. Li. 2015. PRL1 modulates root stem cell niche activity and meristem size through WOX5 and PLTs in Arabidopsis. *Plant J*. 81:399-412.

Jiang, D., and F. Berger. 2017. DNA replication-coupled histone modification maintains Polycomb gene silencing in plants. *Science*. 357:1146-1149.

Kaya, H., K.I. Shibahara, K.I. Taoka, M. Iwabuchi, B. Stillman, and T. Araki. 2001. FASCIATA genes for chromatin assembly factor-1 in arabidopsis maintain the cellular organization of apical meristems. *Cell*. 104:131-142.

Kirik, A., A. Pecinka, E. Wendeler, and B. Reiss. 2006. The chromatin assembly factor subunit FASCIATA1 is involved in homologous recombination in plants. *Plant Cell*. 18:2431-2442.

Kong, X., S. Lu, H. Tian, and Z. Ding. 2015. WOX5 is Shining in the Root Stem Cell Niche. *Trends Plant Sci*. 20:601-603.

Krogan, N.T., X. Yin, W. Ckurshumova, and T. Berleth. 2014. Distinct subclades of Aux/IAA genes are direct targets of ARF5/MP transcriptional regulation. *New Phytol*. 204:474-483.

Larson-Rabin, Z., Z. Li, P.H. Masson, and C.D. Day. 2009. FZR2/CCS52A1 expression is a determinant of endoreduplication and cell expansion in Arabidopsis. *Plant Physiol*. 149:874-884.

Leyser, H.M., and L.J. Furner. 1992. Characterisation of three shoot apical meristem mutants of *Arabidopsis thaliana*. *Development*. 116:397-403.

Liu, Z., Y. Zhu, J. Gao, F. Yu, A. Dong, and W.H. Shen. 2009a. Molecular and reverse genetic characterization of NUCLEOSOME ASSEMBLY PROTEIN1 (NAP1) genes unravels their function in transcription and nucleotide excision repair in Arabidopsis thaliana. *Plant J*. 59:27-38.

Liu, Z.Q., J. Gao, A.W. Dong, and W.H. Shen. 2009b. A truncated Arabidopsis NUCLEOSOME ASSEMBLY PROTEIN 1, AtNAP1;3T, alters plant growth responses to abscisic acid and salt in the Atnap1;3-2 mutant. *Mol Plant*. 2:688-699.

Lloyd, R.S., C.W. Haidle, and D.L. Robberson. 1978. Bleomycin-specific fragmentation of double-stranded DNA. *Biochemistry*. 17:1890-1896.

Mozgova, I., P. Mokros, and J. Fajkus. 2010. Dysfunction of chromatin assembly factor 1 induces shortening of telomeres and loss of 45S rDNA in Arabidopsis thaliana. *Plant Cell*. 22:2768-2780.

Mozgova, I., T. Wildhaber, Q. Liu, E. Abou-Mansour, F. L'Haridon, J.P. Metraux, W. Gruissem, D. Hofius, and L. Hennig. 2015. Chromatin assembly factor CAF-1 represses priming of plant defence response genes. *Nat Plants*. 1:15127.

Muchova, V., S. Amiard, I. Mozgova, M. Dvorackova, M.E. Gallego, C. White, and J. Fajkus. 2015. Homology-dependent repair is involved in 45S rDNA loss in plant CAF-1 mutants. *Plant J*. 81:198-209.

Muller, A., C. Guan, L. Galweiler, P. Tanzler, P. Huijser, A. Marchant, G. Parry, M. Bennett, E. Wisman, and K. Palme. 1998. AtPIN2 defines a locus of Arabidopsis for root gravitropism control. *EMBO J*. 17:6903-6911.

Munoz-Viana, R., T. Wildhaber, M.S. Trejo-Arellano, I. Mozgova, and L. Hennig. 2017. Arabidopsis Chromatin Assembly Factor 1 is required for occupancy and position of a subset of nucleosomes. *Plant J*. 92:363-374.

Ono, T., H. Kaya, S. Takeda, M. Abe, Y. Ogawa, M. Kato, T. Kakutani, O. Mittelsten Scheid, T. Araki, and K. Shibahara. 2006. Chromatin assembly factor 1 ensures the stable maintenance of silent chromatin states in Arabidopsis. *Genes Cells*. 11:153-162.

Otero, S., B. Desvoyes, R. Peiro, and C. Gutierrez. 2016. Histone H3 Dynamics Reveal Domains with Distinct Proliferation Potential in the Arabidopsis Root. *Plant Cell*. 28:1361-1371.

Pecinka, A., H.Q. Dinh, T. Baubec, M. Rosa, N. Lettner, and O. Mittelsten Scheid. 2010. Epigenetic regulation of repetitive elements is attenuated by prolonged heat stress in Arabidopsis. *Plant Cell*. 22:3118-3129.

Pi, L., E. Aichinger, E. van der Graaff, C.I. Llavata-Peris, D. Weijers, L. Hennig, E. Groot, and T. Laux. 2015. Organizer-Derived WOX5 Signal Maintains Root Columella Stem Cells through Chromatin-Mediated Repression of CDF4 Expression. *Dev Cell*. 33:576-588.

Ramirez-Parra, E., and C. Gutierrez. 2007a. E2F regulates FASCIATA1, a chromatin assembly gene whose loss switches on the endocycle and activates gene expression by changing the epigenetic status. *Plant Physiol*. 144:105-120.

Ramirez-Parra, E., and C. Gutierrez. 2007b. The many faces of chromatin assembly factor 1. *Trends Plant Sci*. 12:570-576.

Ransom, M., B.K. Dennehey, and J.K. Tyler. 2010. Chaperoning histones during DNA replication and repair. *Cell*. 140:183-195.

Richards, S., R.H. Wink, and R. Simon. 2015. Mathematical modelling of WOX5- and CLE40-mediated columella stem cell homeostasis in Arabidopsis. *J Exp Bot*. 66:5375-5384.

Sabatini, S., D. Beis, H. Wolkenfelt, J. Murfett, T. Guilfoyle, J. Malamy, P. Benfey, O. Leyser, N. Bechtold, P. Weisbeek, and B. Scheres. 1999. An auxin-dependent distal organizer of pattern and polarity in the Arabidopsis root. *Cell*. 99:463-472.

Sang, Y., C.O. Silva-Ortega, S. Wu, N. Yamaguchi, M.F. Wu, J. Pfluger, C.S. Gillmor, K.L. Gallagher, and D. Wagner. 2012. Mutations in two non-canonical Arabidopsis SWI2/SNF2 chromatin remodeling ATPases cause embryogenesis and stem cell maintenance defects. *Plant J*. 72:1000-1014.

Sarkar, A.K., M. Luijten, S. Miyashima, M. Lenhard, T. Hashimoto, K. Nakajima, B. Scheres, R. Heidstra, and T. Laux. 2007. Conserved factors regulate signalling in Arabidopsis thaliana shoot and root stem cell organizers. *Nature*. 446:811-814.

Sato, A., and K.T. Yamamoto. 2008. Overexpression of the non-canonical Aux/IAA genes causes auxin-related aberrant phenotypes in Arabidopsis. *Physiol Plant*. 133:397-405.

Schonrock, N., V. Exner, A. Probst, W. Gruissem, and L. Hennig. 2006. Functional genomic analysis of CAF-1 mutants in Arabidopsis thaliana. *J Biol Chem*. 281:9560-9568.

Shiloh, Y. 2006. The ATM-mediated DNA-damage response: taking shape. *Trends Biochem Sci*. 31:402-410.

Takatsuka, H., and M. Umeda. 2015. Epigenetic Control of Cell Division and Cell Differentiation in the Root Apex. *Front Plant Sci*. 6:1178.

Truernit, E., H. Bauby, B. Dubreucq, O. Grandjean, J. Runions, J. Barthelemy, and J.C. Palauqui. 2008. High-resolution whole-mount imaging of three-dimensional tissue organization and gene expression enables the study of Phloem development and structure in Arabidopsis. *Plant Cell*. 20:1494-1503.

van den Berg, C., V. Willemsen, G. Hendriks, P. Weisbeek, and B. Scheres. 1997. Short-range control of cell differentiation in the Arabidopsis root meristem. *Nature*. 390:287-289.

Varas, J., E. Sanchez-Moran, G.P. Copenhaver, J.L. Santos, and M. Pradillo. 2015. Analysis of the Relationships between DNA Double-Strand Breaks, Synaptonemal Complex and Crossovers Using the Atfas1-4 Mutant. *PLoS Genet*. 11:e1005301.

Varas, J., J.L. Santos, and M. Pradillo. 2017. The Absence of the Arabidopsis Chaperone Complex CAF-1 Produces Mitotic Chromosome Abnormalities and Changes in the Expression Profiles of Genes Involved in DNA Repair. *Front Plant Sci*. 8:525.

Wang, J., M. Qi, J. Liu, and Y. Zhang. 2015. CARMO: a comprehensive annotation platform for functional exploration of rice multi-omics data. *Plant J*. 83:359-374.

Yu, Y., A. Dong, and W.H. Shen. 2004. Molecular characterization of the tobacco SET domain protein NtSET1 unravels its role in histone methylation, chromatin binding, and segregation. *Plant J*. 40:699-711.

Zhou, W., J. Gao, J. Ma, L. Cao, C. Zhang, Y. Zhu, A. Dong, and W.H. Shen. 2016. Distinct roles of the histone chaperones NAP1 and NRP and the chromatin-remodeling factor INO80 in somatic homologous recombination in Arabidopsis thaliana. *Plant J*. 88:397-410.

Zhou, W., Y. Zhu, A. Dong, and W.H. Shen. 2015. Histone H2A/H2B chaperones: from molecules to chromatin-based functions in plant growth and development. *Plant J*. 83:78-95.

Zhu, Y., A. Dong, D. Meyer, O. Pichon, J.P. Renou, K. Cao, and W.H. Shen. 2006. Arabidopsis NRP1 and NRP2 encode histone chaperones and are required for maintaining postembryonic root growth. *Plant Cell*. 18:2879-2892.

Zhu, Y., A. Dong, and W.H. Shen. 2013. Histone variants and chromatin assembly in plant abiotic stress responses. *Biochim Biophys Acta*. 1819:343-348.

Zhu, Y., L. Rong, Q. Luo, B. Wang, N. Zhou, Y. Yang, C. Zhang, H. Feng, L. Zheng, W.H. Shen, J. Ma, and A. Dong. 2017. The Histone Chaperone NRP1 Interacts with WEREWOLF to Activate GLABRA2 in Arabidopsis Root Hair Development. *Plant Cell*. 29:260-276.

FIGURE LEGENDS

Figure 1. Root growth is inhibited in mutants deprived of the histone chaperones NRPs and/or CAF-1.

A. Seedling phenotypes of wild-type (WT), the mutant deprived of NRP1 and NRP2 (*m56-1*), the mutant deprived of CAF-1 (*fas2-4*), and their combined mutant *m56-1fas2-4* at 12 day-after-germination (DAG). Scale bar = 10 mm.

B. Root growth curves for WT, *m56-1*, *fas2-4* and *m56-1fas2-4* from 4 to 12 DAG. The mean value from 30 plants is shown. Error bars represent standard deviations.

Figure 2. Depletion of NRPs and CAF-1 drastically impairs stem cell proliferation and causes SCN disorganization.

A. Root meristematic zone from tip is reduced in *m56-1* (depleted of NRP1 and NRP2), more severely in *fas2-4* (depleted of CAF-1), and most severely in *m56-1fas2-4* (depleted of NRP1, NRP2 and CAF-1), as compared to wild-type (WT). DIC (Differential Interference Contrast) images were taken on roots at 5 day-after-germination (DAG). Red arrows indicate the transition from meristematic zone to elongation zone. Scale bar = 50 μm.

B. Comparison of root meristem cell number in WT, *m56-1*, *fas2-4*, and *m56-1fas2-4* at 5 DAG. Root meristem cell number was defined as the number of cortex cells in a file extending the quiescent center (QC) to the first elongated cell. The mean value from 30 plants is shown. Error bars represent standard deviations. Statistically significant differences (p <0.05) are as indicated.

C. Root-tip cellular organization in WT, *m56-1*, *fas2-4*, and *m56-1fas2-4*. Confocal images were taken from 5 DAG roots stained using mPS-PI method. The close-up regions are colored for different cell types as following: QC cell in dark blue, columella root cap and columella initial cells in orange, lateral root cap cells in yellow, epidermal cells and epidermis/lateral root cap initials in red-brown, cortex cells in light blue, endodermal cells in dark green, cortex/endodermis initials in light green, and stele cells and stele initials in gray. The question mark indicates where the cell identity is uncertain. Vertical scale bar = 50 μm.

D. Expression pattern of *QC25* and accumulation of starch granules in WT, *m56-1*, *fas2-4* and *m56-1fas2-4* root tips at 5 DAG. DIC images show blue staining of GUS activity from

QC25 expression together with dark grey staining of starch granules by Lugol's solution. Vertical scale bar = 50 μm.

Figure 3. Transcriptome analysis of differentially expressed genes in roots of the mutant plants deprived of the histone chaperones NRPs and/or CAF-1.

A. Number of up-regulated genes and down-regulated genes in *m56-1* (depleted of NRP1 and NRP2), *fas2-4* (depleted of CAF-1) and *m56-1fas2-4* (depleted of NRP1, NRP2 and CAF-1), as compared to the wild-type control.

B. Venn diagram showing overlap of up- or down-regulated genes found in *m56-1fas2-4* with up-regulated genes found in *fas2-4* or *m56-1*. Red asterisk indicates that the overlap among the three mutants is statistically significant (p <0.05).

C. Venn diagram showing overlap of up- or down-regulated genes found in *m56-1fas2-4* with down-regulated genes found in *fas2-4* or *m56-1*. Asterisk indicates that the overlap among the three mutants is statistically significant (p <0.05).

D. K-means clustering of transcriptomic changes in *m56-1*, *fas2-4* and *m56-1fas2-4*. The numbers in the brackets indicate the numbers of genes found in each of the eight clusters. The color range representing Log2 value is shown at the bottom of graph.

E. Gene ontology (GO) analysis of up-regulated genes from clusters 1 and 2 (red), and down-regulated genes from clusters 7 and 8 (green), for distribution of number of genes belonging to different biological function categories as indicated.

Figure 4. Expression and chromatin change of some key root regulatory genes in mutants deprived of the histone chaperones NRPs and/or CAF-1.

A. Relative gene expression levels determined by quantitative RT-PCR analysis. RT-PCR was performed using gene-specific primers and normalized using *ACTIN2* as reference. Relative expression levels of the indicated genes in the *m56-1* (depleted of NRP1 and NRP2), *fas2-4*(depleted of CAF-1) and *m56-1fas2-4* (depleted of NRP1, NRP2 and CAF-1) mutants compared to the wild-type (WT) control (setting as 1) are shown as means ± SD from three biological repeats. Asterisk indicates significant difference compared to WT (p <0.01).

B. ChIP analysis of H3, H3ac and H4ac levels at chromatin of the indicated genes in the *m56-1*, *fas2-4* and *m56-1fas2-4* mutants as compared to WT (setting as 1). Mean ± SD from three biological repeats are shown. Asterisk indicates significant difference between the mutant and WT (p <0.01).

C. Expression pattern of *WOX5:GFP* in WT， *m56-1, fas2-4* and *m56-1fas2-4* roots. Bar = 50μm.

D. Expression pattern of *pSCR:SCR-GFP* in WT, *m56-1, fas2-4* and *m56-1fas2-4* roots. Bar = 50 μm.

E. Expression pattern of *DR5rev:GFP* in WT, *m56-1, fas2-4* and *m56-1fas2-4* roots. Bar = 50 μm.

Figure 5. Analysis of root cell expansion and cell cycle defects in mutants deprived of the histone chaperones NRPs and/or CAF-1.

A. Evaluation of root epidermal cell expansion rate in the *m56-1* (depleted of NRP1 and NRP2), *fas2-4* (depleted of CAF-1) and *m56-1fas2-4* (depleted of NRP1, NRP2 and CAF-1) mutants as compared to the wild-type (WT) control. Cell size was measured along the distance from proximal to distal of the quiescent center (QC) of roots at 5 day-after-germination (DAG). Regression lines are included: R^2 = 0.933 (WT), 0.9066 (*m56-1*), 0.9505 (*fas2-4*) and 0.9424 (*m56-1fas2-4*). The statistical significance of regression was estimated from the F-test (F < 0.001) in all regression analyses.

B. DNA ploidy distribution in WT, *m56-1*, *fas2-4* and *m56-1fas2-4* roots at 5 DAG. Significant differences of pairwise comparisons are indicated (* p <0.05, ** p <0.01).

C. Expression pattern of *CYCB1;1:GUS* in WT, *m56-1*, *fas2-4* and *m56-1fas2-4* roots at 5 DAG. Bar = 50 μm.

D. Relative expression levels of cell cycle and DNA repair genes determined by quantitative RT-PCR analysis. RT-PCR was performed using gene-specific primers and normalized using *ACTIN2* as reference. Relative expression levels of the indicated genes in the *m56-1*, *fas2-4* and *m56-1fas2-4*mutants compared to the wild-type control (setting as 1) are shown as means ± SD from three biological repeats. Asterisk indicates significant difference compared to WT (p <0.01).

Figure 6. Analysis of root cell death in mutants deprived of the histone chaperones NRPs and/or CAF-1.

A. PI-stained root tips of wild-type (WT), *m56-1* (depleted of NRP1 and NRP2), *fas2-4* (depleted of CAF-1), *m56-1fas2-4* (depleted of NRP1, NRP2 and CAF-1), *atm-2* (depleted of ATM), *atm-2m56-1fas2-4* (depleted of ATM, NRP1, NRP2 and CAF-1), *atr-2* (depleted of ATR), and *atr-2m56-1fas2-4* (depleted of ATR, NRP1, NRP2 and CAF-1) at 5 day-after-germination (DAG). Bar = 50 μm.

B. Percentage of roots displaying cell death and total area size of dead cells per root in WT and mutants as indicated. Data shown are means ± SE (n = 50).

Figure 7. Analysis of H2A phosphorylation (γ- H2AX) in mutants deprived of the histone chaperones NRPs and/or CAF-1.

A. Whole-mount root immunofluorescence staining analysis of wild-type (WT), *m56-1* (depleted of NRP1 and NRP2), *fas2-4* (depleted of CAF-1), *m56-1fas2-4* (depleted of NRP1, NRP2 and CAF-1), *atm-2* (depleted of ATM), *atm-2m56-1fas2-4* (depleted of ATM, NRP1, NRP2 and CAF-1), *atr-2* (depleted of ATR), and *atr-2m56-1fas2-4* (depleted of ATR, NRP1, NRP2 and CAF-1) at 5 day-after-germination (DAG). The γ- H2AX signal detected using specific antibodies is shown in red and DNA staining by DAPI (4',6-diamidino-2-phenylindole) is shown in blue. Bar = 50 μm.

B-D. Western blot analysis of H3, H2A and γ-H2A.X levels in WT and the indicated mutants under normal plant growth conditions. Coomassie Brilliant Blue staining gel (CBB) and ACTIN blot (@ACTIN) are shown as loading and internal controls. Numbers under panels indicate relative signal intensity after normalization to ACTIN (**B**) or H3 (**C** and **D**), and represent means ± SD from three biological repeats.

E-G. Western blot analysis of H3, H2A and γ-H2A.X levels in WT and the indicated mutants under bleomycin-treated plant growth conditions. CBB and ACTIN are shown as loading and internal controls. Numbers under panels indicate relative signal intensity after normalization to ACTIN (**E**) or H3 (**F** and **G**), and represent means ± SD from three biological repeats.

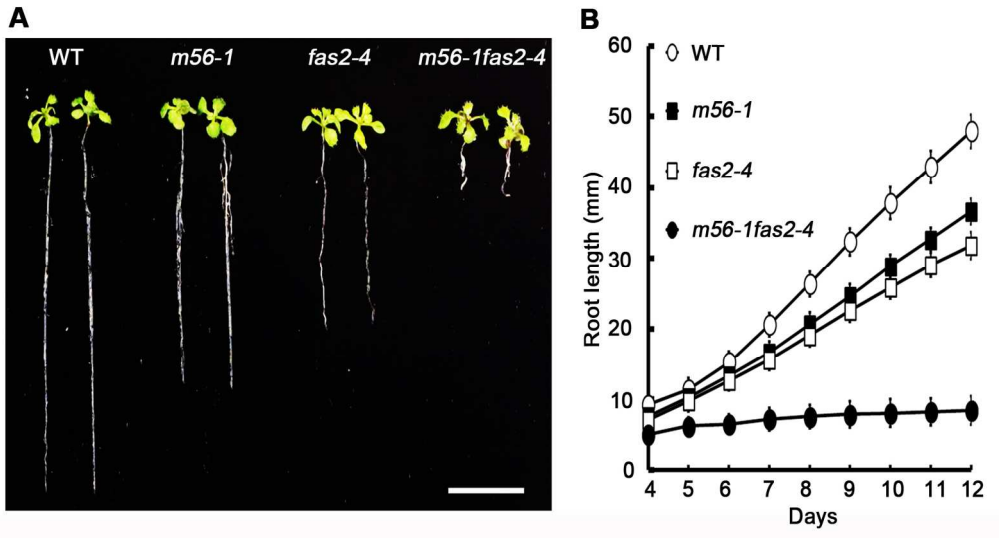

Figure 1

160x86mm (300 x 300 DPI)

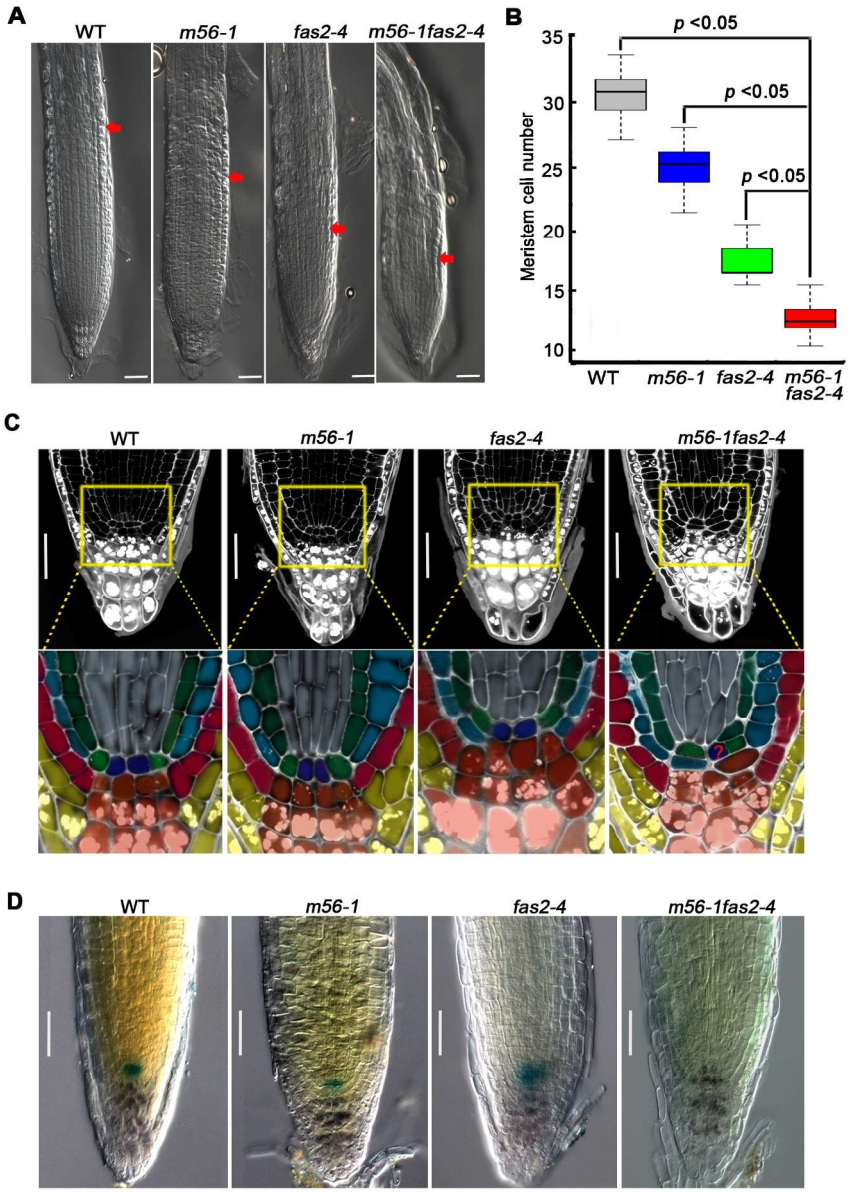

Figure 2

160x222mm (300 x 300 DPI)

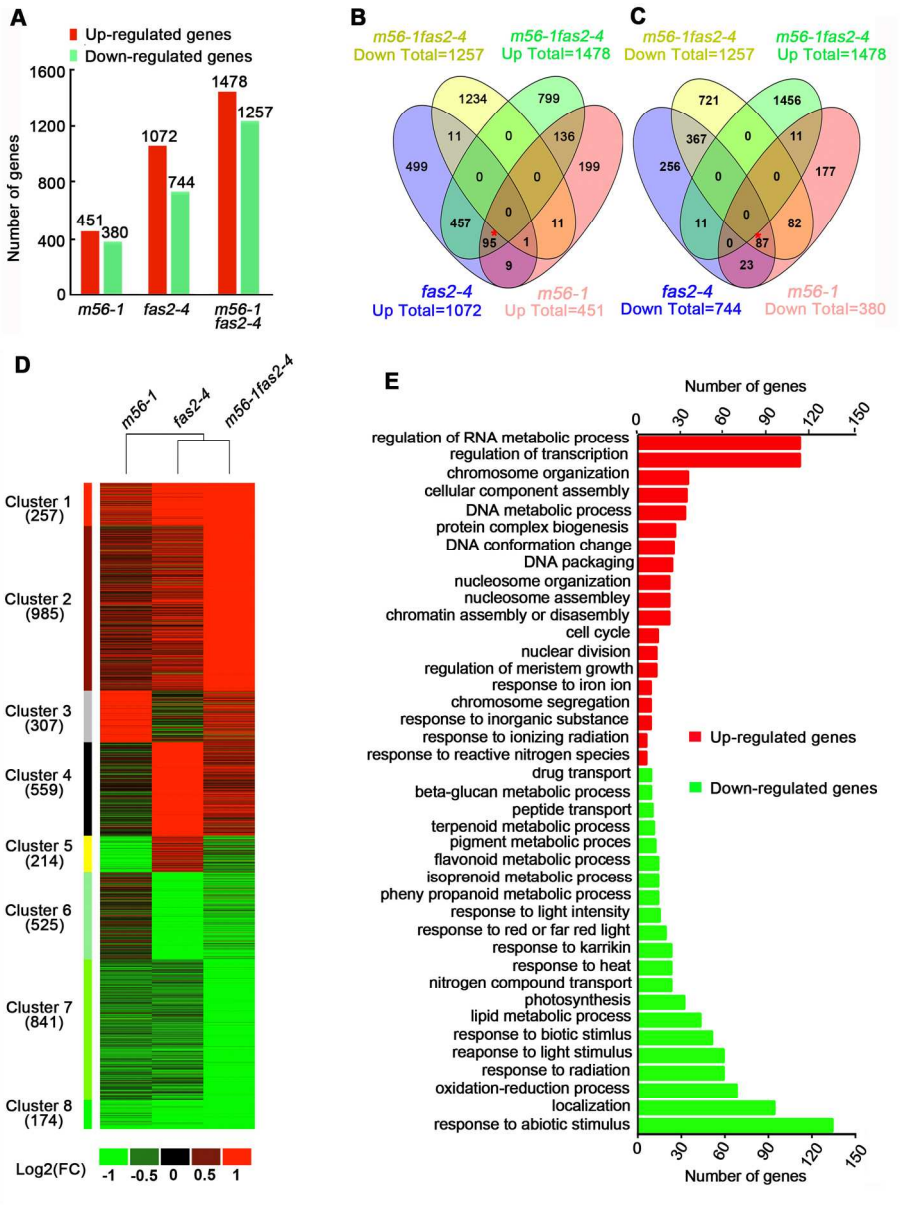

Figure 3

170x226mm (300 x 300 DPI)

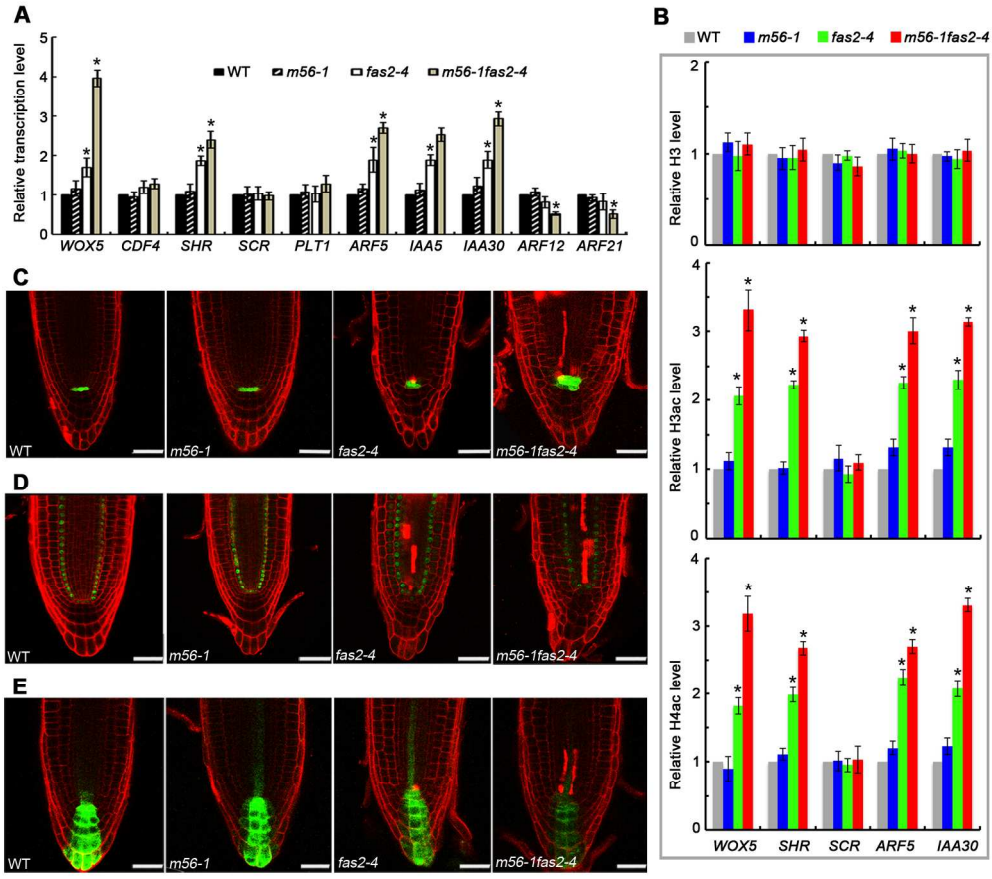

Figure 4

180x159mm (300 x 300 DPI)

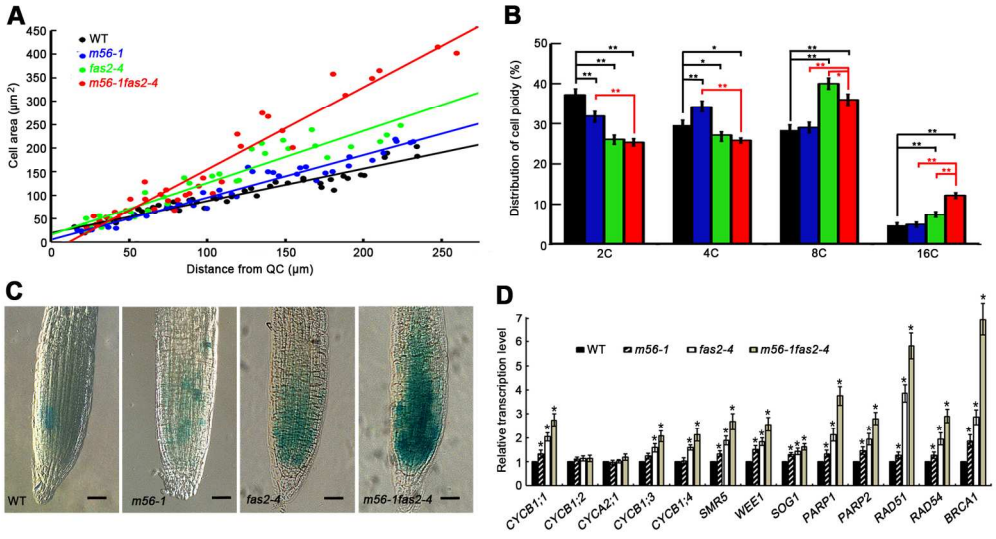

Figure 5

170x91mm (300 x 300 DPI)

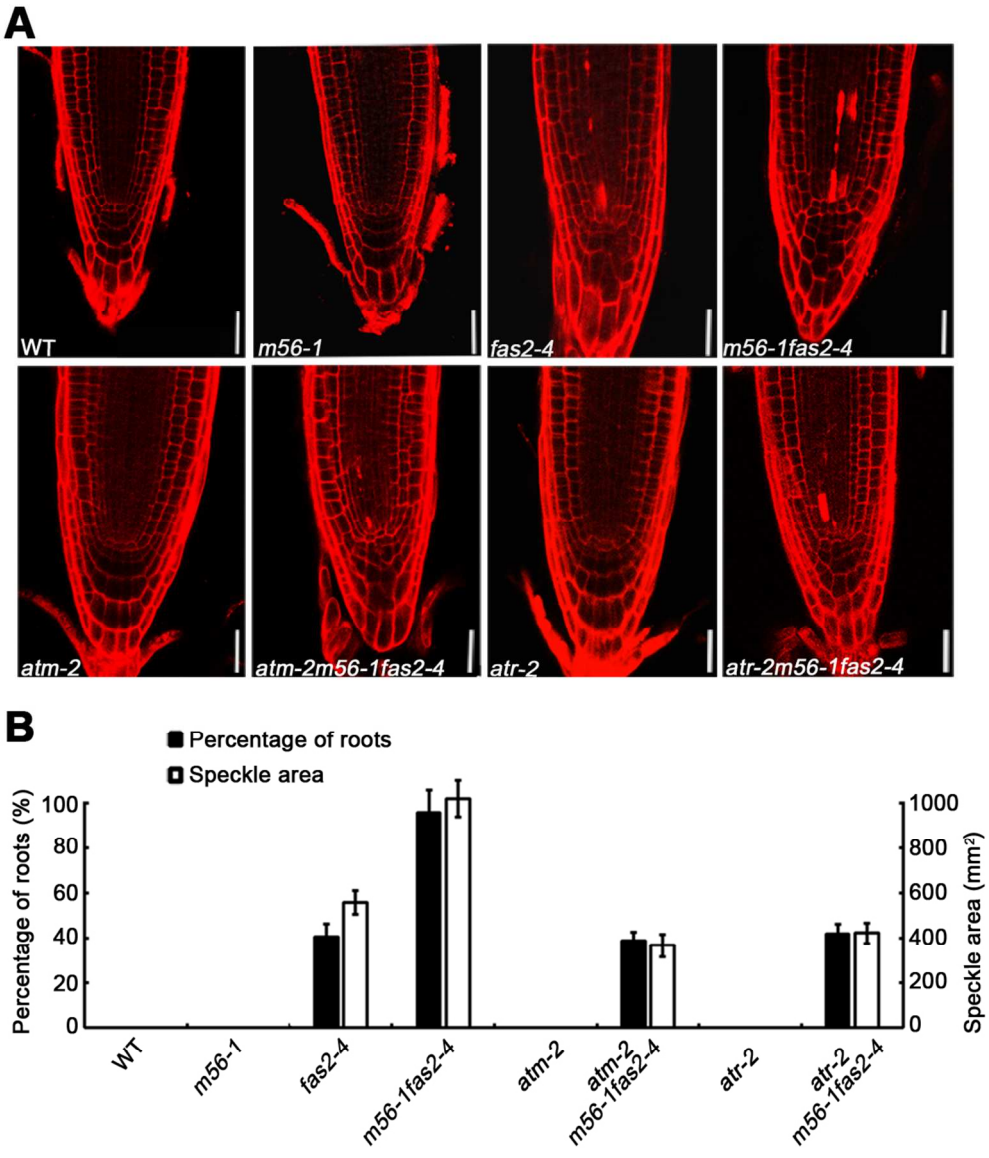

Figure 6

99x115mm (300 x 300 DPI)

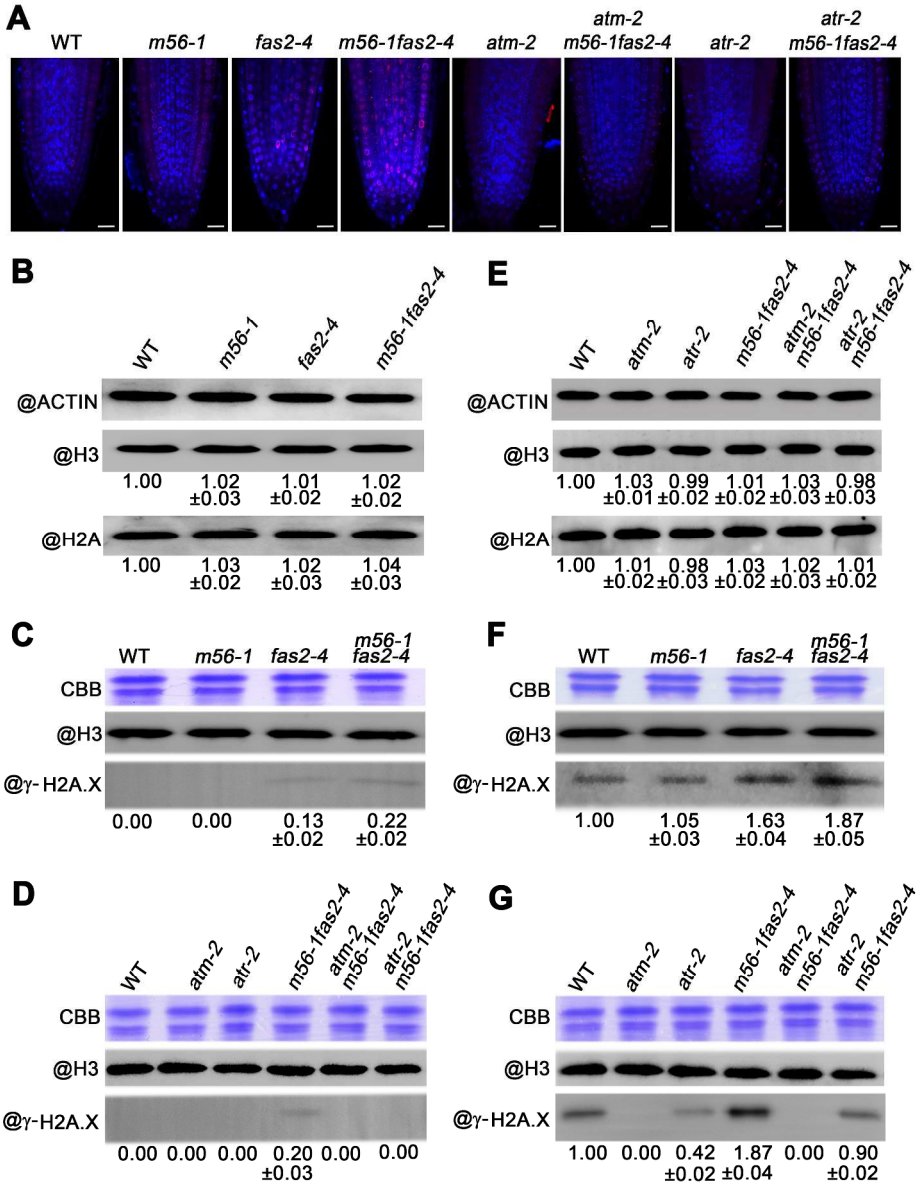

Figure 7

299x389mm (300 x 300 DPI)

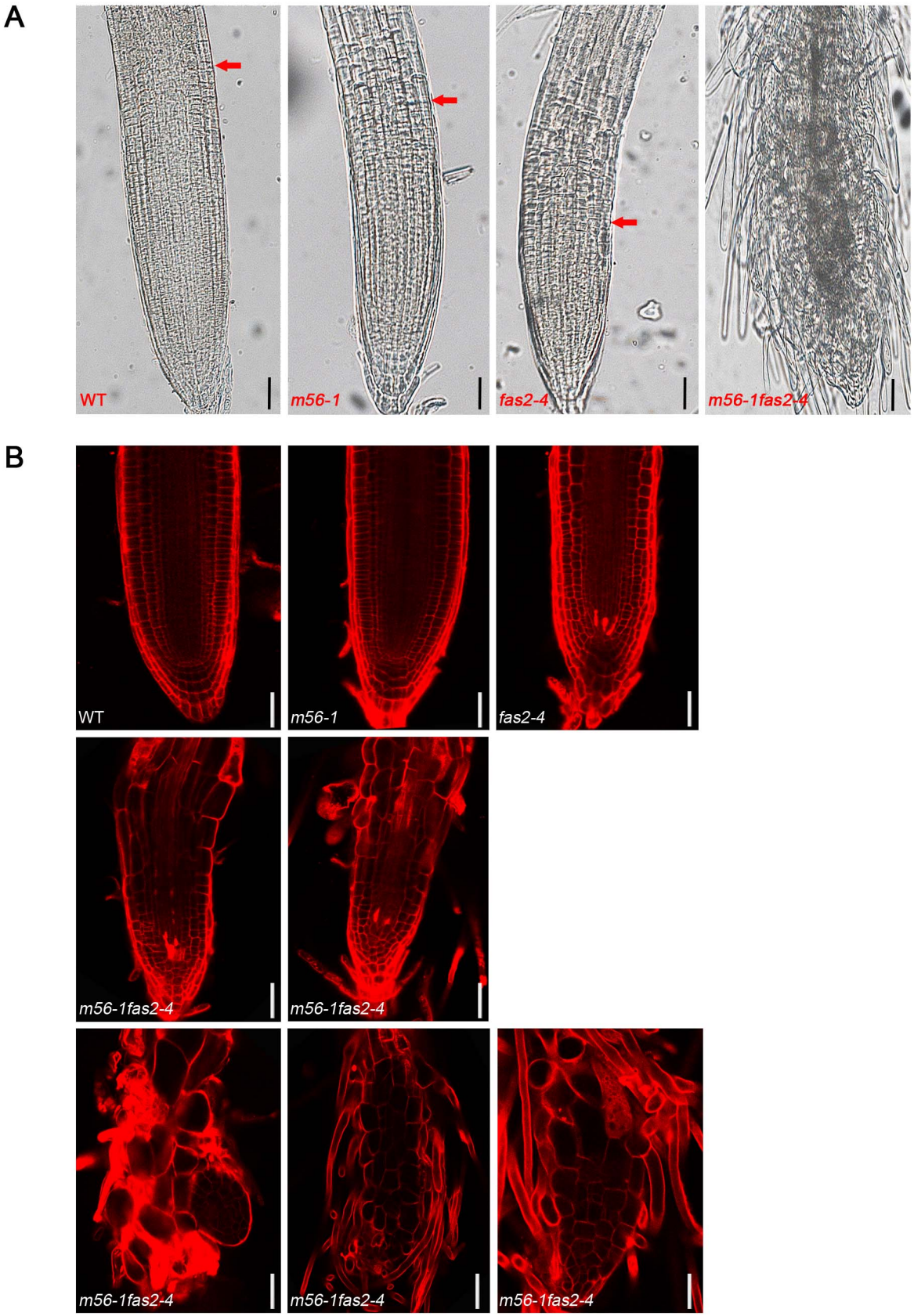

Supplemental Figure S1. Root phenotype analysis showing drastically disorganization of root apex in the *m56-1fas2-4* mutant.

A. Representative root tips of wild-type (WT) and mutants *m56-1* (depleted of NRP1 and NRP2), *fas2-4* (depleted of CAF-1) and *m56-1fas2-4* (depleted of NRP1, NRP2 and CAF-1) at 15 day-after-germination (DAG). Arrows indicate the transition from meristematic zone to elongation zone. Note that the meristem zone of *m56-1fas2-4* is barely observed and the root tip is mostly occupied by root hairs. Bar=50 μm.

B. PI-stained root tips of WT, *m56-1*, *fas2-4* and *m56-1fas2-4* at 15 DAG. Middle panels represent weak phenotypes and bottom panels represent strong phenotypes of the *m56-1fas2-4* mutant. Bar=50 μm.

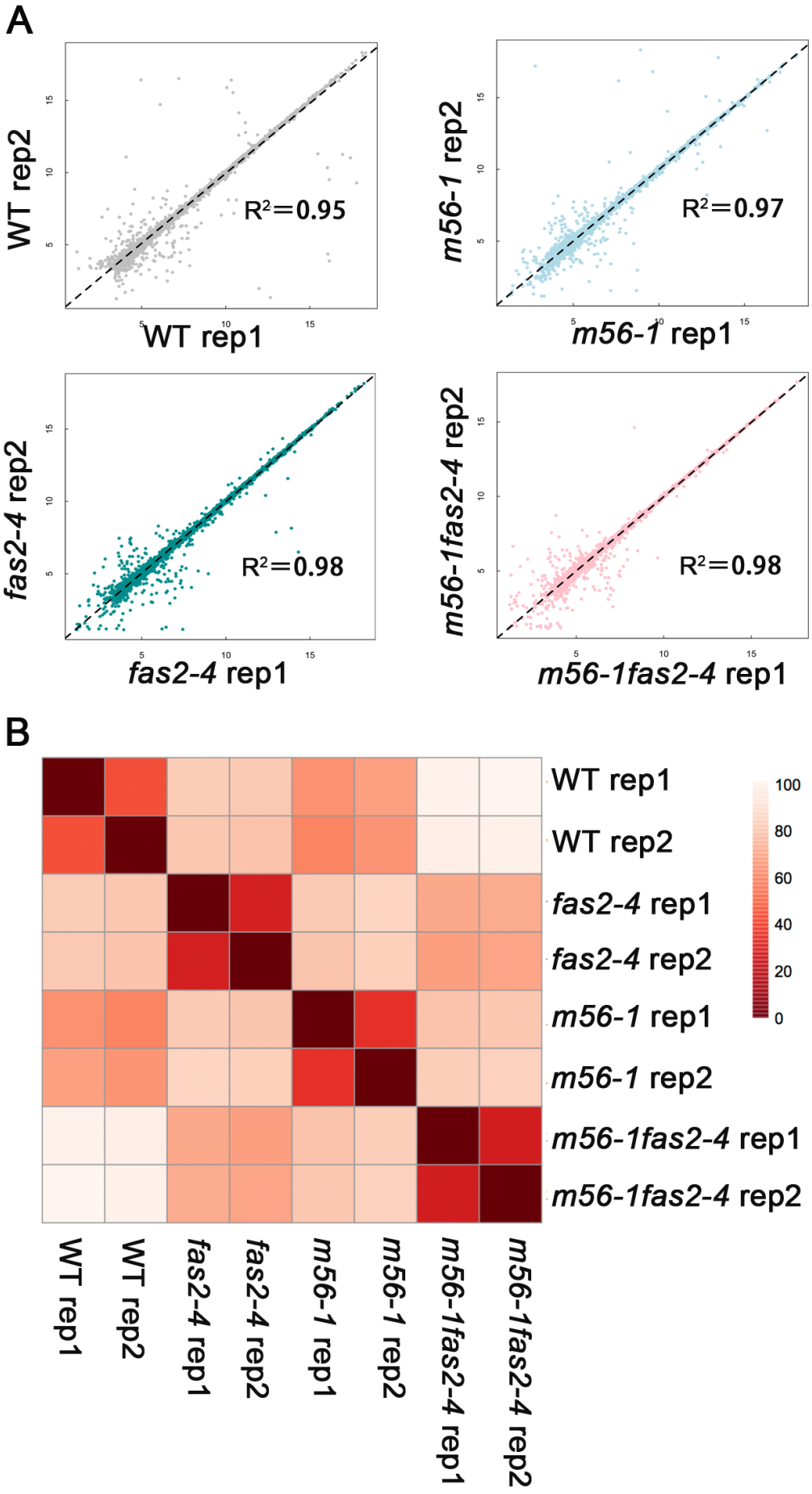

Supplemental Figure S2. Comparisons of microarray data sets obtained in this study.

A. Scatterplot of microarray replicate comparisons in wild-type (WT) and mutants *m56-1* (depleted of NRP1 and NRP2), *fas2-4* (depleted of CAF-1) and *m56-1fas2-4* (depleted of NRP1, NRP2 and CAF-1).

B. Heatmap of correlationship among all analyzed samples. Euclidean distance is used to represent relationship. The darker the red color shows, the closer relationship between two samples exists.

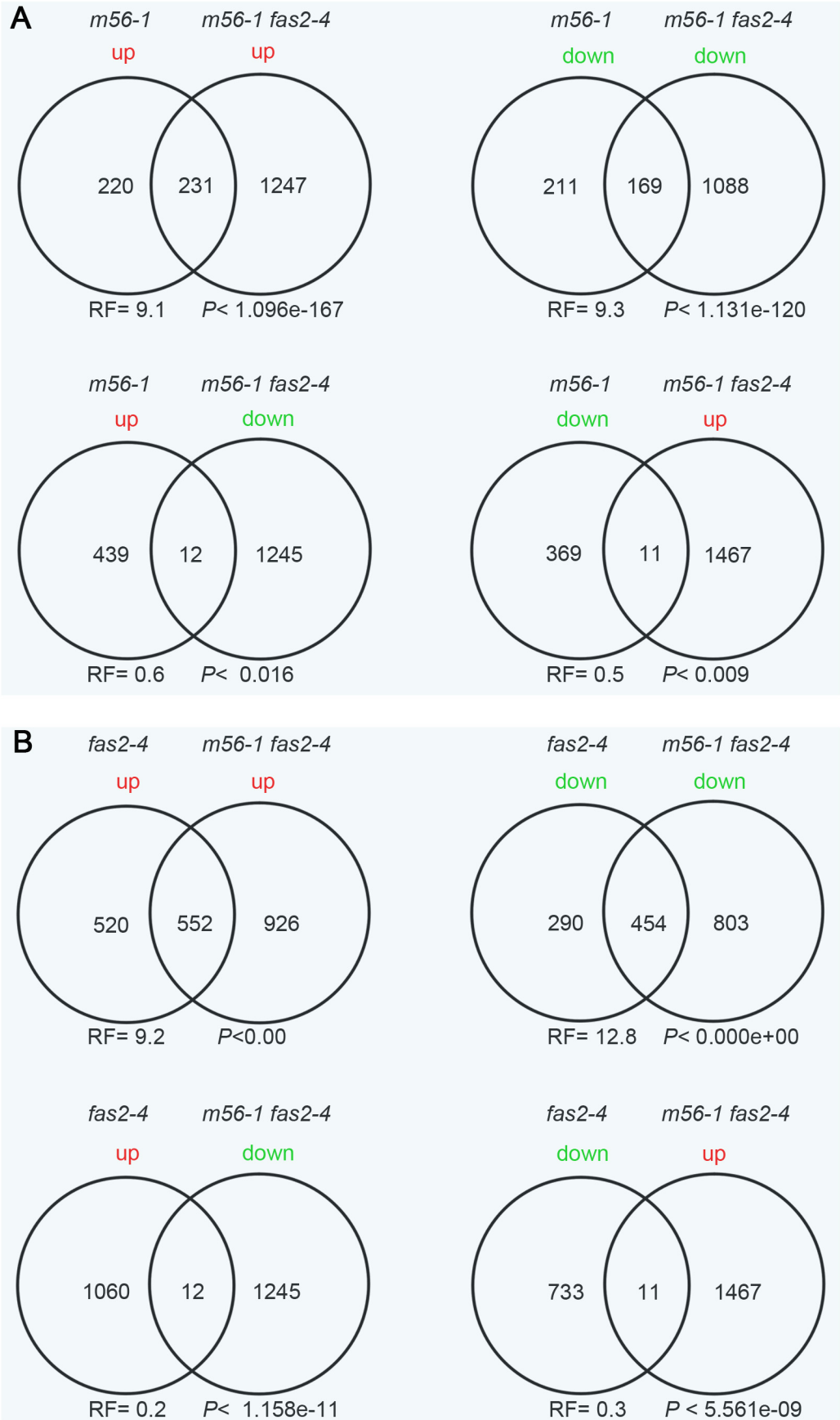

Supplemental Figure S3. Venn diagrams showing pairwise overlap together with statistic significance assessment on lists of differentially expressed genes between the *m56-1fas2-4* and *m56-1* (A) or *fas2-4* (B) mutants.

Hypergeometric test was based on a total number of 26277 Arabidopsis genes. Representation factor (RF) superior to 1 together with *p*-value inferior to 0.05 indicates a significant overlap higher than expected between two groups at random.

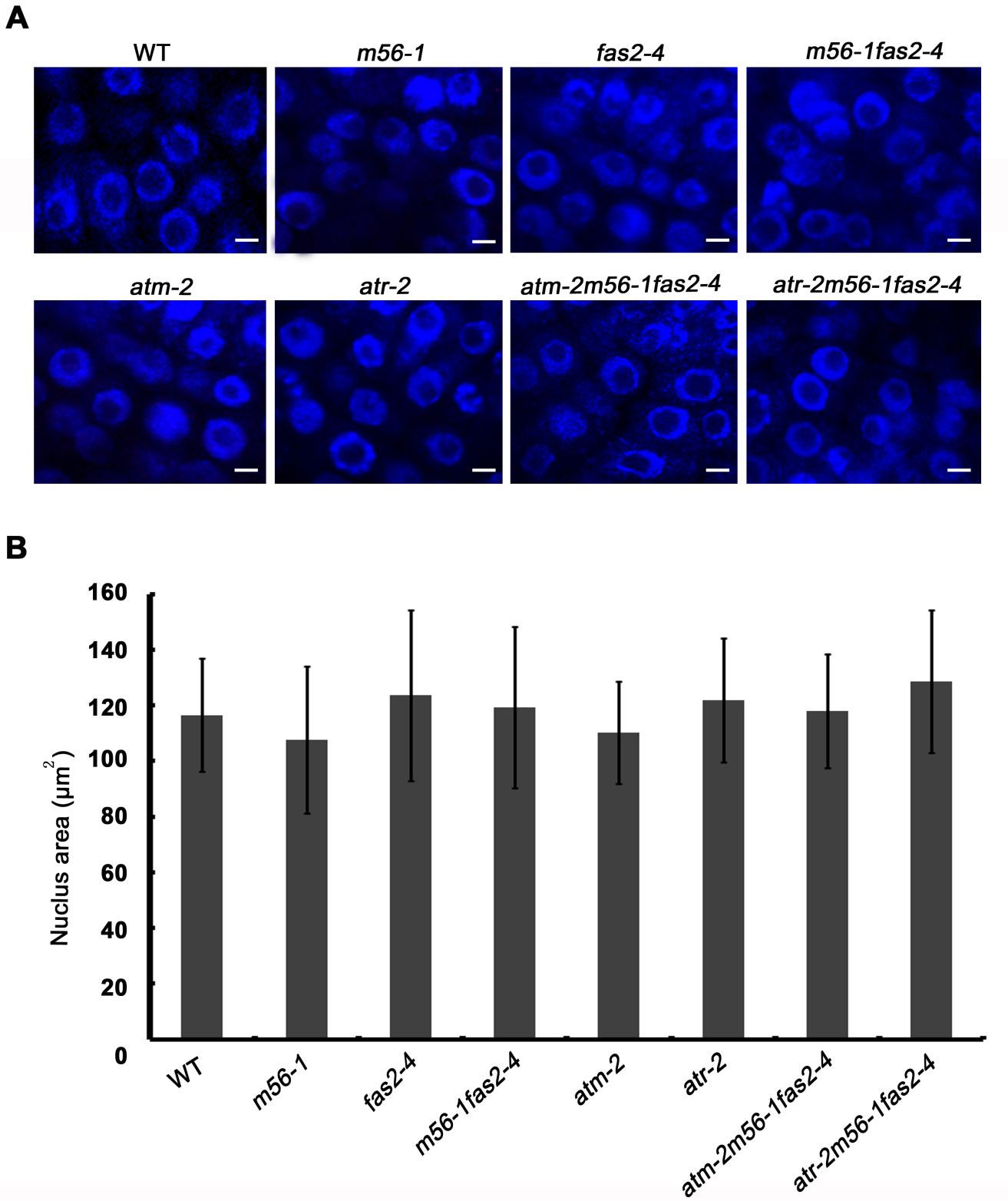

Supplemental Figure S4. DAPI-staining analysis of nuclei of cells around QC in WT and in the *m56-1*, *fas2-4*, and *m56-1fas2-4* mutants.

A. Representative images showing cells of wild-type (WT) and the *m56-1* (deprived of NRP1 and NRP2), *fas2-4* (deprived of CAF-1), *m56-1fas2-4* (deprived of NRP1, NRP2 and CAF-1), *atm-2* (deprived of ATM), *atr-2* (deprived of ATR), *atm-2m56-1fas2-4* (deprived of ATM, NRP1, NRP2 and CAF-1), and *atr-2m56-1fas2-4* (deprived of ATM, NRP1, NRP2 and CAF-1) mutants from seedlings at 5 day-after-germination (DAG). DAPI staining is shown in blue color. Scale bar = 5 μm.

B. Comparison of nuclear area from the cells of WT and those of the different mutants. The mean value from about 10 cells per root from 10 5-DAG-seedlings is shown together with an error bar representing the standard deviation.

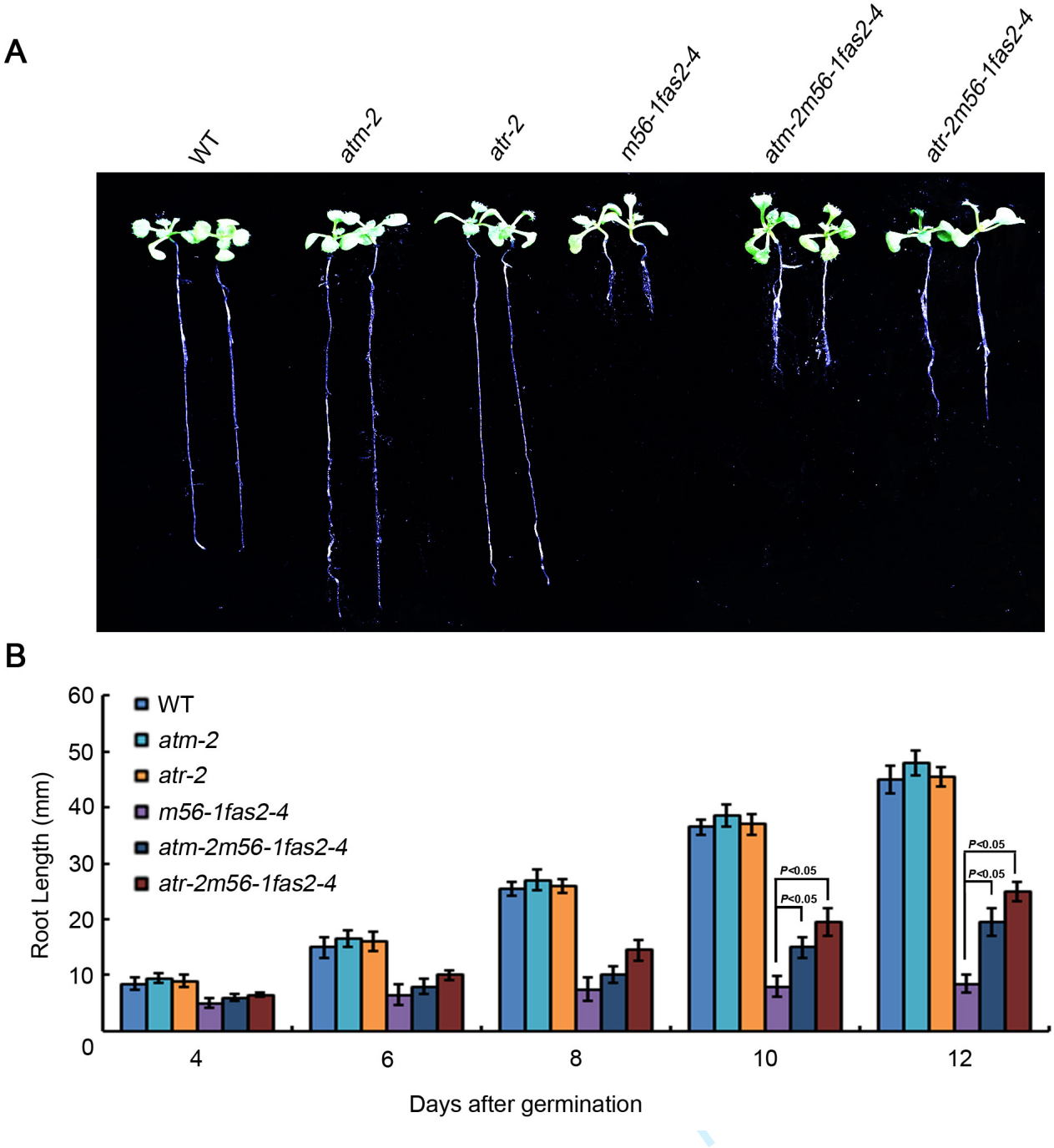

Supplemental Figure S5. Loss of *ATM* or *ATR* partially rescues the short root phenotype of the *m56-1fas2-4* mutant.

A. Phenotypes of wild-type (WT) and the *atm-2* (deprived of ATM), *atr-2* (deprived of ATR), *m56-1fas2-4* (deprived of NRP1, NRP2 and CAF-1), *atm-2m56-1fas2-4* (deprived of ATM, NRP1, NRP2 and CAF-1), and *atr-2m56-1fas2-4* (deprived of ATM, NRP1, NRP2 and CAF-1) mutants at 12 day-after-germination (DAG). Scale bar = 10 mm.

B. Comparison of root length of WT and the *atm-2*, *atr-2*, *m56-1fas2-4*, *atm-2m56-1fas2-4*, *atr-2m56-1fas2-4* mutants from 4 to 12 DAG. The mean value from 30 plants is shown. Error bars represent standard deviations.

Table S1. List of primers used in this study.

Gene name	Primer Name	Sequence
Primers for genotyping		
nrp1-1	N5-G-LP	ATGTGTTATCTTTGGGCTCCC
	N5-G-RP	TGAACTCTCTGGAAGTGGAGG
nrp2-1	N6-G-LP	CAACTCCAATAAATCAACCGTTG
	N6-G-RP	CGATTGAGAGGACAAGCTCTG
fas2-4	FAS2-G-LP	CATTCGTTTTTCTCCATCTGG
	FAS2-G-RP	AGGTGACCATGACAATCTTCG
atm-2	ATM-G-LP	TGTGGTTCAGTCTTGCCTCCCAGA
	ATM-G-RP	CGGTCACCGTTTGCCAAAGCCA
	ATM-G-126	TCTCTCCTTGTTTCAAGCTCTGC
atr-2	ATR-G-LP	GCAGCAAAAATTTCTTGGTTGG
	ATR-G-RP	GGGTTCCGATGTTCAAAGTGTG
LB	LBa1	TGGTTCACGTAGTGGGCCATCG
	LBb1.3	ATTTTGCCGATTTCGGAAC
Primers for RT-PCR		
WOX5	WOX5-LP	CGAGCCGGTCTTAGAACTCC
	WOX5-RP	TTCTGCCTCTCCCTAGCCT
CDF4	CDF4-LP	TCGGAAGTCCAAACCACCTG
	CDF4-FP	TCGACTTGGCGAACACCATT
SHR	SHR-LP	ACGGAGCAATCTTGGAAGCA
	SHR-RP	CTTGTTGGCCACGACAACT
SCR	SCR-LP	GCCTGCCTTTTGAGTTCTGC
	SCR-RP	AGAGTGTGTGCATCAGAGCC
PLT1	PLT1-LP	AGTGGGAGCTACAACACTGC
	PLT1-RP	GGTTCCATCACTGGAAGGCA
ARF5	ARF5-LP	GCTCCCAACTTGAGGGAGAC
	ARF5-RP	ACCTTGCTTGAAGAGATGAAGC
IAA5	IAA5-LP	TCTTGCACGATCCAAGGAACA
	IAA5-RP	GCTCTGCAAATTCTGTTCGGA
IAA30	IAA30-LP	CCCAAGGAACATCTCCAACCA
	IAA30-RP	ACTCTCGACTACATGTTCAATGCT
ARF12	ARF12-LP	ATTCATCGGAGAGGCAACAC
	ARF12-RP	CAAGAACAAGCGTTTACGAGAAGT
ARF21	ARF21-LP	TCCTTGTGTCAATATAGGAGGCA
	ARF21-RP	CTGCGTTAAATGTTCCGCGA
CYCB1;1	CYCB1;1- LP	TAAGCAGATTCAGTTCCGGTCAAC
	CYCB1;1- RP	GGGAGCTTTACGAAAGAAATACTCC
CYCB1;2	CYCB1;1- LP	TAAGCAGATTCAGTTCCGGTCAAC
	CYCB1;1- RP	GGGAGCTTTACGAAAGAAATACTCC
CYCA2;1	CYCA2;1- LP	GCCGCTCAAGCGTCTGATAAGG
	CYCA2;1- RP	GCTGAAGCGGCAATTAGGGATG
CYCB1;3	CYCB1;3-LP	AGCTTGTAGGTGTTAGTGCT T
	CYCB1;3-RP	GTTCATGTCAAGTTTGATCTC
CYCB1;4	CYCB1;4-LP	ATGAGATCGATTCTGATAGA
	CYCB1;4-RP	GCTAACAATGAACTGGCTGCTG
SMR5	SMR5-LP	TTCTTCGGTGGTTCCCGGAG

SMR5	SMR5-RP	CGGAGATACGGTGACGGTTG
WEE1	WEE1-LP	TCCCCCATCACCTCATCTGT
	WEE1-RP	GTCGCCAGGAGAGTTTCACA
SOG1	SOG1-LP	CTGTCTTATGCCAGCGCACA
	SOG1-RP	ACCAGGTGTTAAGAGTGATGGG
PARP1	PARP1-LP	GTCGAATCTGGAGCAGGGAG
	PARP1-RP	GGCCTTCAGGCTTGGAGAAT
PARP2	PARP2-LP	AGCACAAAAGGTGTGGGGAA
	PARP2-RP	GAACGTTCCACTGGTTTGCC
RAD51	RAD51-LP	AGCAGGTATTGCTTCTGTTGATGT
	RAD51-RP	TCAACCTTGGCATCACTAATTCCT
RAD54	RAD54-LP	AACTCCGGTTGTGGTTGCTTTA
	RAD54-RP	AGTTGTTACATTGCTCATTCCATCTT
BRCA1	BRCA1-LP	TGAAGCTGATGGGAAGCAGG
	BRCA1-RP	GTTTCTCGGTGGGACTTCGT

Primers for ChIP-PCR

WOX5	WOX5-FP	GGGAGGAGAGGTTTTCGAGT
	WOX5-RP	CTGCAAAGATCAGTCTCTCCCA
SHR	SHR-FP	CGCTTCAAGAAGGACCGAGT
	SHR-RP	CGGCCACCATAATGACCCTT
SCR	SCR-FP	TAACATTCCGACCACCACGG
	SCR-RP	ACAACCACCGTCTCTTACGG
ARF5	ARF5-FP	ACACAAAGTTACCTGCTCGCT
	ARF5-RP	CAGGCCCTTTGGTGTGTCTC
IAA30	IAA30-FP	CATCATTTCCTCTGCCGCAC
	IAA30-RP	CCTAAGCACGGACCTGAGAC